Diagnostics of Chemical Oxygen-Iodine Lasers Energized by Singlet Oxygen Jet-Generators

Contract F61708-96-C0005

SPC 96-4078

Final Report

Principal Investigator:
Professor Salman Rosenwaks

Department of Physics, Ben-Gurion University of the Negev
Beer-Sheva 84105, Israel

December 1998

ABSTRACT

We have carried out diagnostic measurements in a small-scale supersonic chemical oxygen iodine laser (COIL) with transonic mixing, energized by a singlet oxygen jet-generator (JSOG). Using three diode laser based diagnostic systems for oxygen, water and iodine, we measured the $O_2(^1\Delta)$ yield and water vapor fraction at the exit of the JSOG and the gain in the resonator. In addition the chlorine utilization and gas temperature at the JSOG exit were measured. For conditions corresponding to the maximum chemical efficiency of the supersonic COIL energized by the JSOG, the $O_2(^1\Delta)$ yield, water vapor fraction, chlorine utilization and temperature at the JSOG exit are 0.65, 0.08, 0.92 and 30 C, respectively. Increase of the basic hydrogen peroxide temperature results in increase of the water vapor fraction caused by increase of the saturated water vapor pressure in the generator. As the pressure in the generator rises from 18 to 60 Torr the yield decreases from 0.65 to 0.48. The dependence of the yield on the generator pressure is consistent with a rate constant of the $O_2(^1\Delta)$ energy pooling reaction of 2.7×10^{-17} cm^3s^{-1}. The same rate constant explains the measured variation of the temperature along the flow in the diagnostic cell. The small signal gain and the temperature at the resonator optical axis are 0.25 %/cm and 280 K, respectively. The enclosed papers describe these measurements. The first is a summary of the work on all three diagnostic systems whereas the second describes in detail the work on water and oxygen.

s

REPORT DOCUMENTATION PAGE

Form Approved OMB No. 0704-0

1. AGENCY USE ONLY (Leave blank)	2. REPORT DATE	3. REPORT TYPE AND DATES COVERED
	December 1998	Final Report

4. TITLE AND SUBTITLE

Diagnostics Of Chemical Oxygen-Iodine Lasers Energized By Singlet Oxygen Jet-Generators

5. FUNDING NUMBERS

F6170896C0005

6. AUTHOR(S)

Dr. Prof. Salman Rosenwaks

7. PERFORMING ORGANIZATION NAME(S) AND ADDRESS(ES)

Ben-Gurion University of the Negev
PO Box 653
Beer-Sheva 84 105
Israel

8. PERFORMING ORGANIZATION REPORT NUMBER

N/A

9. SPONSORING/MONITORING AGENCY NAME(S) AND ADDRESS(ES)

EOARD
PSC 802 BOX 14
FPO 09499-0200

10. SPONSORING/MONITORING AGENCY REPORT NUMBER

SPC 96-4078

11. SUPPLEMENTARY NOTES

12a. DISTRIBUTION/AVAILABILITY STATEMENT

Approved for public release; distribution is unlimited.

12b. DISTRIBUTION CODE

A

13. ABSTRACT (Maximum 200 words)

This report results from a contract tasking Ben-Gurion University of the Negev as follows: The contractor will carry out diagnostic measurements in a small-scale supersonic chemical oxygen-iodine laser (COIL) with transonic mixing, energized by a singlet oxygen jet-generator (JSOG). They will use a three diode laser-based diagnostic system for oxygen, water, and iodine and measure the oxygen singlet yield and water vapor fraction at the exit of the JSOG and the gain in the resonator.

14. SUBJECT TERMS

EOARD

15. NUMBER OF PAGES

32

16. PRICE CODE

N/A

17. SECURITY CLASSIFICATION OF REPORT	18. SECURITY CLASSIFICATION OF THIS PAGE	19, SECURITY CLASSIFICATION OF ABSTRACT	20. LIMITATION OF ABSTRACT
UNCLASSIFIED	UNCLASSIFIED	UNCLASSIFIED	UL

To be published in SPIE (1999)

Chemical Oxygen Iodine Laser investigations in Israel

B. D. Barmashenko, D. Furman and S. Rosenwaks
Department of Physics, Ben-Gurion University of the Negev, Beer-Sheva 84105, Israel

ABSTRACT

We report on diagnostic measurements in a small scale supersonic chemical oxygen iodine laser (COIL) with transonic mixing. Using diode laser based diagnostics we measured the $O_2(^1\Delta)$ yield and water vapor fraction at the exit of a jet type singlet oxygen generator (JSOG) and the gain in the resonator. In addition the chlorine utilization and gas temperature at the generator exit were measured. For conditions corresponding to the maximum chemical efficiency of the supersonic COIL energized by the JSOG the $O_2(^1\Delta)$ yield, water vapor fraction, chlorine utilization and temperature at the generator exit are 0.65, 0.08, 0.92 and 30 C. Small signal gain and temperature at the resonator optical axis are 0.25 %/cm and 280 K, respectively. Dependence of the yield on the generator pressure and variation of the temperature along the flow in the diagnostic cell are consistent with rate constant of the $O_2(^1\Delta)$ energy pooling reaction of 2.7×10^{-17} cm^3s^{-1}.

Keywords: chemical lasers, supersonic lasers, oxygen, iodine, power lasers.

1. INTRODUCTION

A 5-cm gain length supersonic chemical oxygen iodine laser (COIL) has been developed recently at Ben-Gurion University for operation at maximum chlorine flow rate of 20 mmole/s [1]. The laser is energized by a jet type singlet oxygen generator (JSOG), operating without buffer gas and applying simple nozzle geometry and transonic mixing of iodine and oxygen. Output power of 190 W with chemical efficiency of 18% was obtained for Cl_2 flow rate of 11.8 mmole/s [1].

To optimize the output power and understand the kinetic and mixing processes in the laser medium it is necessary to measure the small signal gain and number densities of different species in the flow. This is done using diagnostic techniques developed by Physical Sciences Inc. [2]. The diagnostics include three separate systems able to monitor water vapor, ground state oxygen, iodine atoms and temperature. Each system is based on sensitive absorption spectroscopy by tunable near infrared diode lasers. Using the diagnostics we measured important parameters of the COIL: the yield of $O_2(^1\Delta)$ after the chemical generator, water vapor fraction in the flow and the gain in the resonator. In addition the chlorine utilization and gas temperature at the generator exit are measured.

2. EXPERIMENTAL SETUP

The JSOG used to produce $O_2(^1\Delta)$ is the same as described in [1]. Basic hydrogen peroxide (BHP) is prepared from 3 L 50% wt H_2O_2 + 2.5 L 55% wt KOH (6.5 M HO_2^- and 3.3 M H_2O_2 in excess) and kept at -20°C. The jets back pressure [1] is 1.6 atm which corresponds to BHP flow rate of ~ 0.3 L/s. An exit valve is used to regulate the gas pressure in the reaction zone of the JSOG. Most of the Cl_2 reacts with the BHP to produce singlet oxygen. The oxygen flows through the exit valve to a diagnostic cell which serves as an interface between the generator and an iodine injectors housing. The cell is 14 cm long in the flow direction with a 5 cm x 1 cm flow cross section. It is equipped with two ports for pressure measurements, two ports for temperature measurements and three interfaces for optical absorption measurements. These identical optical interfaces are used for the chlorine, oxygen and water vapor absorption measurements. The location of the optical axes of the interfaces are 7.5, 11.5 and 15.5 cm downstream of the generator exit, while the temperatures ports are located at 9.5 and 13.5 cm. The $O_2(^1\Delta)$ yield, water vapor density and Cl_2 utilization in the jet-type generator are simultaneously measured in the diagnostic cell.

The iodine-oxygen mixing system, consisting of 10 rectangular supersonic nozzles, is the same as in [1]. The iodine is injected perpendicular to the primary flow in its transonic section. The laser section starts at the nozzle exit plane (flow cross section of 5 x 1 cm^2), and then the floor and the ceiling of the section diverge at an angle of 8°. The optical resonator is 28.5 cm long and has 5 cm active length. For the gain diagnostic system we replace the laser mirrors with a suitable interface for gain diagnostic. The gain was measured at the optical axis of the resonator, 4.5 cm downstream of the nozzle exit plane.

The water diagnostic is based on a diode laser system, which scans an individual rovibrational line of the water v_1+v_3 band in the 1.39-μm region. The laser beam is split to signal and reference beams; the signal is passed through a 5 cm path length in the diagnostic cell and compared with the reference beam. Under our conditions, this system is able to measure water molecules number densities as low as 10^{15} cm^{-3}.

The oxygen diagnostic system measures oxygen ground state ($O_2(^3\Sigma)$) density and then the density of $O_2(^1\Delta)$ is inferred. The measurements are made using a diode laser that scans over a line of the $O_2(^3\Sigma) \rightarrow O_2(^1\Sigma)$ transition around 760 nm. Like in the water system the laser beam is split to reference and signal. However, since the absorption is very weak, the signal beam is passed 21 times through the 5-cm-width diagnostic cell, in a multi-pass Herriott cell configuration [3]. The beams are then compared by a balanced radiometric detector (BRD) which amplifies the logarithm of the ratio between the reference and the signal. The diagnostics is calibrated in the beginning and end of every experimental run by measuring the area under the absorption line in medical-grade oxygen (99.5% minimum) at pressures from 1 to 6 Torr. The diagnostic is able to measure oxygen number densities as low as 6×10^{15} cm^{-3}. For the JSOG experiments the error in the yield is estimated to be ± 0.05.

The iodine diagnostic system monitors gain for the $I^*(5p^5\ ^2P_{1/2}, F=3) \rightarrow I(5p^5\ ^2P_{3/2}, F = 4)$ transition at 1315 nm. The laser frequency is scanned over the I transition in a single pass configuration through the gain region in the resonator. The gain sensitivity is 10^{-2} %/cm.

The chlorine utilization in the JSOG is found from the number density of unreacted Cl_2 in the diagnostic cell, the pressure and the temperature. The density of Cl_2 is determined by measuring the absorption at 340 nm. The chlorine density measurement system consists of a stabilized tungsten-halogen lamp (power stability is 0.05%), chopper, fiber optics, 350nm filter and a lock-in amplifier in a conventional, single beam configuration.

3. RESULTS AND DISCUSSION

A. Chlorine utilization

Chlorine utilization vs. residence time of the gas in the generator is plotted in Fig. 1. The residence time is estimated using the known cross section and length of the reaction zone, the measured chlorine flow at the generator inlet, the partial Cl_2+O_2 gas pressure and gas temperature. The Cl_2+O_2 partial pressure is calculated from the measured gas pressure in the generator (we neglect gas pressure gradient in the generator) and the water fraction in the generator. The water fraction is assumed to be the same as the water fraction in the diagnostic cell (see below in section 3 B).

Fig. 1 includes data from many experiments with different chlorine flow rates and generator gas pressures. It is seen that the utilization is usually higher than 0.9 and slowly increases with residence time. For standard operating conditions corresponding to maximum laser power in the experiments [1] (11.7 mmole/s of chlorine, 20 Torr in the generator and residence time of 6 ms) the utilization is 0.92 ± 0.01.

The utilization decreases from 0.92 to 0.88 as the chlorine flow rate increases from 11.7 mmole/s to 20 mmole/s without changing the generator outlet cross section (the opening of the exit valve). This effect can be explained by the increase of the gas velocity in the generator with chlorine flow rate due to the decrease in boundary layer thickness resulting from the pressure increase. Velocity increase results in decrease of the gas residence time in the reaction zone, and hence in decrease of the utilization (see Fig. 1).

B. Water vapor

Water vapor density was measured in the diagnostic cell. The water vapor partial pressure in the generator can be calculated assuming that the water vapor fraction in the diagnostic cell is the same as in the generator. Fig. 2 shows the generator total pressure and the water vapor partial pressure in an experimental run in which the generator total pressure was changed by adjusting the generator exit valve. The relative change in the water vapor partial pressure is much smaller than the change in the total pressure. In addition, the water vapor pressure tends to stabilize, with time, in some equilibrium pressure. It is concluded that under steady state conditions the water vapor partial pressure is close to saturation.

As the BHP bulk temperature was let to rise with time (simply by turning off the cooling), the water vapor pressure in the generator increased. Comparison between the temperature dependencies of the measured water vapor pressure and calculated saturated water vapor pressure above BHP (presented in [4]), showed that the "effective" temperature of the jet surface is six to seven degrees higher than the measured bulk temperature. The temperature of the jets is expected to be

higher than the bulk temperature because of heat exchange in the gear pump and transport line, and because of the jet surface reactions.

Fig. 3 summarizes the results of many experimental runs. The water vapor fraction in the flow is plotted against the generator total pressure, for BHP temperature between –16°C to -18°C (the water vapor partial pressure weakly depends on the temperature in this range). The accuracy of measurement of each experimental point is much better than the scattering of the points in the graph. The explanation for the scattering is that during many experiments it was possible to see, in the diagnostic cell, some amount of liquid being carried by the flowing gas out of the generator. In that instant the water vapor density (and fraction) was noticed to rise considerably. For standard operating conditions (see section 3A) and dry diagnostic cell, the water vapor fraction was 0.08 ± 0.01.

C. Yield

The yield is plotted in Fig. 4 as a function of the generator Cl_2+O_2 partial pressure, which was found as described in section 3A. In some experiments the ground state oxygen diagnostics was positioned 4 cm upstream of the center of the diagnostic cell, in the others 4 cm downstream. There is not much difference in these two sets of results. This is in agreement with energy loss computations (Chi analysis [5]) that take into account the pooling reaction

$$O_2(^1\Delta) + O_2(^1\Delta) \rightarrow O_2(^1\Sigma) + O_2(^3\Sigma). \qquad (1)$$

The figure shows also two calculated curves which were obtained using surface chemistry model (referred also as "well stirred limit" model) [6] where depletion of HO_2^- ions near the gas-liquid interface is neglected and only gas-phase losses of $O_2(^1\Delta)$ in the pooling reaction (1) are taken into account. The model has two fitting parameters: the chlorine lifetime in the JSOG, τ, and detachment yield, Y_0. The values of τ and Y_0 were chosen to fit the measured utilization and yield at Cl_2+O_2 partial pressure of 18 Torr (corresponding to total pressure of 20 Torr). Pressure dependencies of Y are calculated for two different values of the rate constant k_p of $O_2(^1\Delta)$ deactivation. The first value, 2.7×10^{-17} cm^3/s [7], is the rate constant of reaction (1), whereas the second value, 6.1×10^{-17} cm^3/s [8], is the effective rate constant of $O_2(^1\Delta)$ deactivation taking into account both reaction (1) and the reaction $O_2(^1\Delta) + O_2(^1\Delta) \rightarrow 2O_2(^3\Sigma)$. It is seen that using the lower rate, 2.7×10^{-17} cm^3/s, in the calculations gives better agreement with experimental results. The yield measured for standard operation conditions (see section 3A) is 0.65 ± 0.05.

The yield slightly increases as the chlorine flow rate increases (without changing the generator outlet cross section). A possible reason is lower pooling losses, as the decrease in gas residence time more than compensates for the increase in oxygen density.

D. Temperature

Fig. 5 shows the behavior of the temperature measured in two points along the flow (see section 2). Until the 200th second the diagnostic cell pressure was changed (at the 40th, 80th, 125th second), without changing Cl_2 flow rate. This was achieved by injecting N_2 downstream of the diagnostic cell (through the iodine-oxygen mixing system) and choking the flow. It is seen that the temperature and the temperature difference increase in the diagnostic cell with the cell pressure. After the 200th second, when we increased the chlorine flow rate, there was a minor increase in temperature. At the 260th second we increased the cell pressure again.

Neglecting heat transfer from the gas to the walls of the diagnostic cell and the change of the yield Y along the flow in the cell (see discussion of Fig. 4), the gas temperature is given by

$$T = T_i + \chi_T k_P Y^2, \qquad (2)$$

where T_i is the temperature at the generator exit,

$$\chi_T = \frac{q_\Delta}{c_P}\left(\frac{p}{kT_{AV}}\right)^2 \frac{n_{O2}{}^2 V}{n^3} \qquad (3)$$

is a modified "chi" factor (definition of the usual "chi" factor is given in [5]), q_Δ is the energy of $O_2(^1\Delta)$, $c_p = 7/2$ k is the heat capacity of diatomic gas, $T_{AV} = 0.5(T+T_i)$ is the average temperature, n_{O2} and n are the oxygen and total flow rates, respectively, and V is the volume over which the losses are calculated.

Fitting a linear graph to the plot of temperatures as a function of modified chi factor, with T_i equal to T as first iteration gives the slope $k_P Y^2$ and a better intercept T_i (Fig. 6). The points are plotted for different flow rates and temperature measurement positions using the appropriate values of volume (from the generator exit to the measuring position) and flow rate. The slope (after several iteration of T_i) is 1.2×10^{-17} cm^3 s^{-1} °C. Using the measured value of the yield, 0.65 ± 0.05, we get an $O_2(^1\Delta)$ deactivation rate of $(2.8 \pm 0.5) \times 10^{-17} cm^3 s^{-1}$. This value is in agreement with the pooling reaction rate constant $k_p = 2.7 \times 10^{-17}$ cm^3/s rather than with the effective rate constant $k_p = 6.1 \times 10^{-17}$ cm^3/s (see discussion in section IV C).

The temperature at the generator exit is found by extrapolation of the temperatures measured at the two points along the flow. For standard conditions it is about 30 C and increases to 50 C as the generator pressure increases to 60 Torr. The temperature is much higher than the BHP temperature, which means that the gas in the generator is not in thermal equilibrium with the BHP jets, due to heat release caused by $O_2(^1\Delta)$ deactivation.

E. Gain and temperature in the resonator

Fig. 7 shows dependencies of the gain and temperature in the resonator on iodine flow rate. Maximum gain of 0.34%/cm is achieved for iodine flow rate of 0.27 mmole/s which is higher than the flow rate corresponding to the maximum power (0.15 mmole/s) [1]. For iodine flow corresponding to the maximum power (0.15 mmole/s) the gain is 0.25%/cm which is in agreement with value estimated in [1]. The temperature strongly increases with iodine flow rate from 230 K for zero iodine flow to 340 K for 0.4 mmole/s of iodine.

4. CONCLUSIONS

Using diode laser based diagnostics we measured the $O_2(^1\Delta)$ yield and water vapor fraction at the exit of the JSOG and the gain in the resonator. In addition, the chlorine utilization and gas temperature at the generator exit were measured. For conditions corresponding to the maximum chemical efficiency of the COIL [1] (12 mmole/s of chlorine, 20 Torr in the generator and BHP temperature of -17 C) the yield, water vapor fraction and utilization are 0.65, 0.08 and 0.92, respectively. The gas temperature at the generator exit is about 30 C. Absolute error of the yield measurements is estimated to be ± 0.05.

For the above flow conditions, the small signal gain and temperature at the resonator optical axis are 0.25 %/cm and 280 K, respectively (for 1.35 mmole/s of secondary N_2 and 0.15 mmole/s of iodine corresponding to the maximum chemical efficiency). As the iodine flow rate increases from 0 to 0.4 mmole/s the temperature increases from 230 K to 340 K.

As the pressure in the generator rises (for constant chlorine flow rate) the yield and water vapor fraction decrease, whereas chlorine utilization and gas temperature at the generator exit increase. The decrease of the yield is not large: when the $Cl_2 + O_2$ partial pressure increases from 18 to 60 Torr the yield decreases from 0.65 to 0.48. The dependence of the yield on the generator pressure is consistent with rate constant of the pooling reaction (2) of 2.7×10^{-17} $cm^3 s^{-1}$ [7]. The same rate constant explains the measured variation of the temperature along the flow in the diagnostic cell.

Increase of the chlorine flow rate (for constant opening of the generator exit valve) results in a weak increase of the yield and decrease of the chlorine utilization. The generator efficiency defined as the product of the yield and utilization is almost independent of the chlorine flow.

Increase of the BHP temperature results in increase of the water vapor fraction caused by increase of the saturated water vapor pressure in the generator, the yield and utilization being independent of the temperature.

The parameters found in this paper are very useful for parametric studies related to high power COILs and for predicting the output power and gain.

5. REFERENCES

1. D. Furman, B. D. Barmashenko and S. Rosenwaks, "Parametric study of an efficient supersonic chemical oxygen-iodine laser/jet generator system operating without buffer gas," *IEEE J. Quantum Electronics*, vol. 34, pp.1068-1074, 1998.
2. M. G. Allen, K. L. Carleton, S. J. Davis, W. J. Kessler and K. R. McManus, "Diode laser-based messurements of Water vapor and ground state oxygen in chemical oxygen iodine lasers," in *25th AIAA Plasmadynamics and Lasers Conf.*, Colorado Springs, CO, June 20-23, 1994, paper 94-2433.
3. H. J. Baker, "Multifold resonators," in *The Physics and Technology of Laser Resonators*, Ed. by D. R. Hall and P. E. Jackson, Bristol: Inst. of Physics, 1992.
4. M. V. Zagidullin, V. I. Igoshin, V. A. Katulin and N. L. Kupriyanov, "Possibility of operation of a chemical oxygen-iodine laser without a cooled trap," *Sov. J. Quantum Electron.*, vol.13, pp. 75 - 76, 1983.
5. T. L. Rittenhouse, S. P. Phipps, C. A. Helms and K. A. Truesdell, "High efficiency operation of a 5-cm gain length supersonic chemical oxygen-iodine laser," *SPIE*, vol. 2702, pp.333 - 338, 1996.
6. D. A. Copeland, W. E. McDermott, V. Quan and A. H. Bauer, "Exact and approximate solutions of the utilization and yield equations for $O_2(^1\Delta)$ generators," in *24th AIAA Plasmadynamics and Lasers Conf.*, Orlando, FL, July 6 - 9, 1993, paper 93-3220.
7. H. V. Lilenfeld, P. A. G. Carr and F. E. Hovis, "Energy pooling reactions in the oxygen-iodine system," *J. Chem. Phys.*, vol.81, pp. 5730 - 5736, 1984.
8. G. P. Perram and G. D. Hager, "The standard chemical oxygen-iodine laser kinetics package," U.S. Air Force Weapons Lab., AFWL-TR-88-50, Kirtland AFB, NM, Oct. 1988.

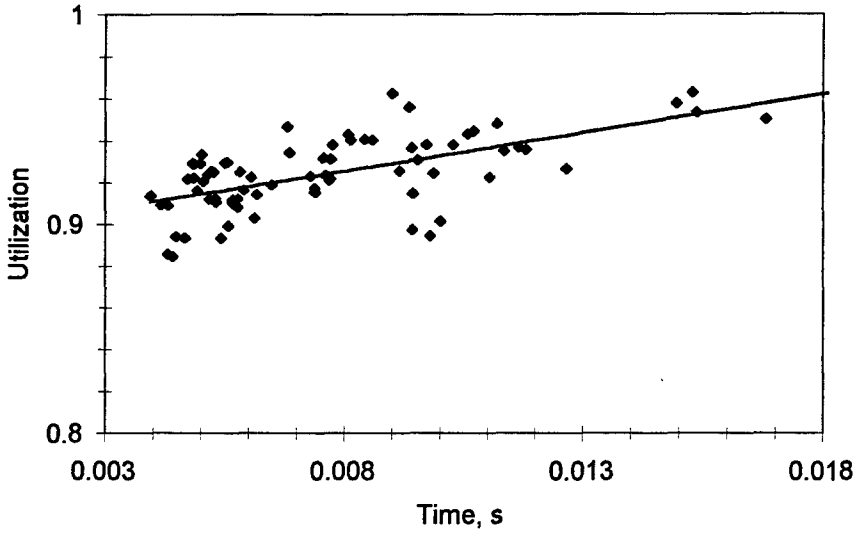

Fig. 1: Chlorine utilization vs. residence time. The data points are from many experiments with different chlorine flow rates (10 to 20 mmole/s) and generator gas pressures (15 to 80 Torr).

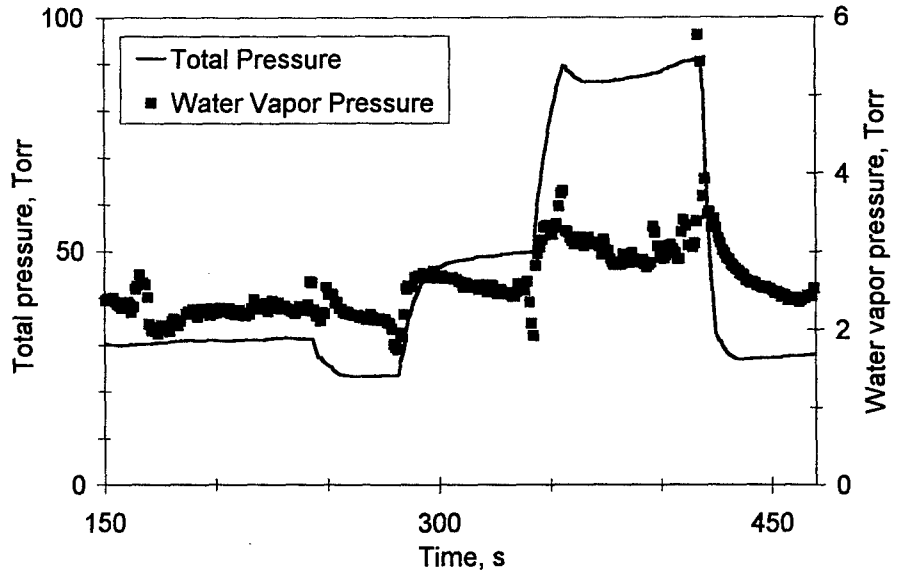

Fig. 2: Total and water vapor pressures in the generator, plotted against time. The data is from a single experimental run with chlorine flow rate of ~10 mmole/s. Changing the generator outlet cross section changed the total pressure.

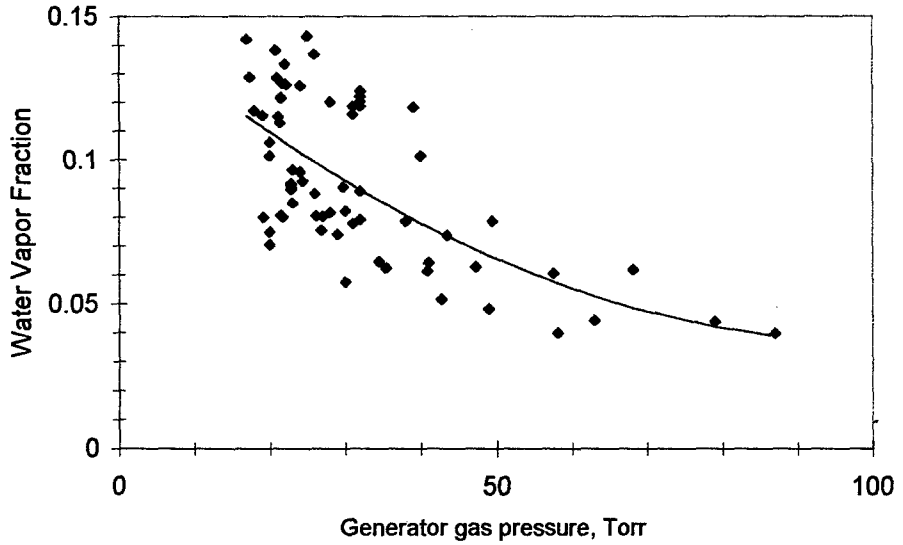

Fig. 3: Water vapor fraction vs. generator gas pressure, for chlorine flow rates between 10 and 12 mmole/s. The graph includes data from experimental runs where liquid droplets were carried out into the diagnostics duct which explains large scattering of the experimental points.

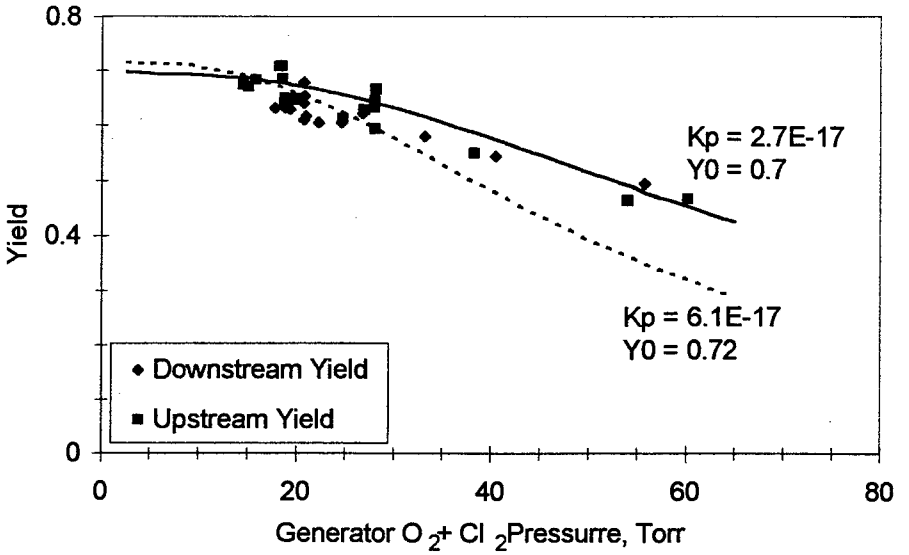

Fig. 4: Yield vs. generator gas pressure for two different positions of the oxygen diagnostics (upstream and downstream) and chlorine flow rate of 12 mmole/s. The lines represent calculations of surface reaction model with two different energy pooling reaction rates. The detachment yield Y_0 and the chlorine lifetime were set so that the calculations will match the measurements at ~18 Torr (corresponding to total pressure of 20 Torr).

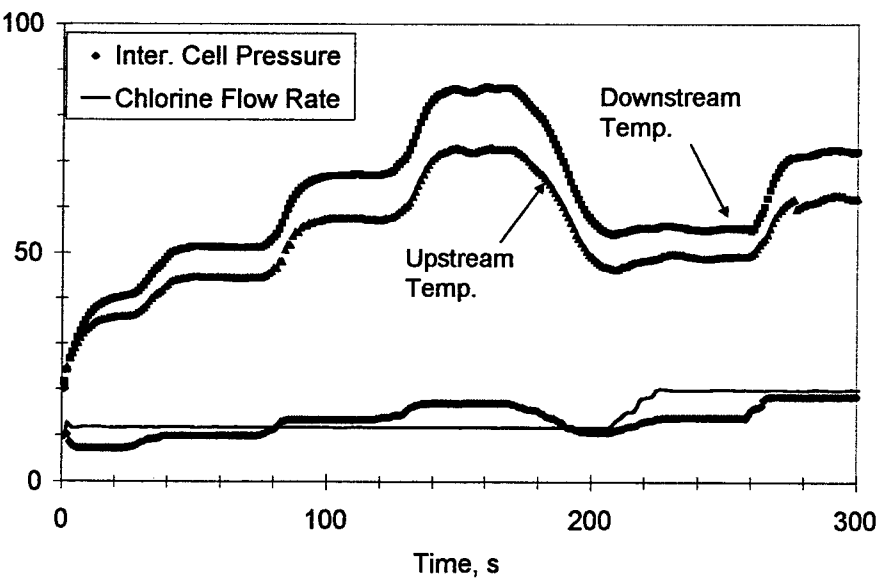

Fig. 5: Upstream and downstream temperatures (degrees Celsius) in a typical experimental run. The diagnostics cell pressure (Torr) was manually changed by choking the flow downstream the cell. At the 200th second the chlorine flow rate (mmole/s) was increased, note that the temperature was not significantly increased.

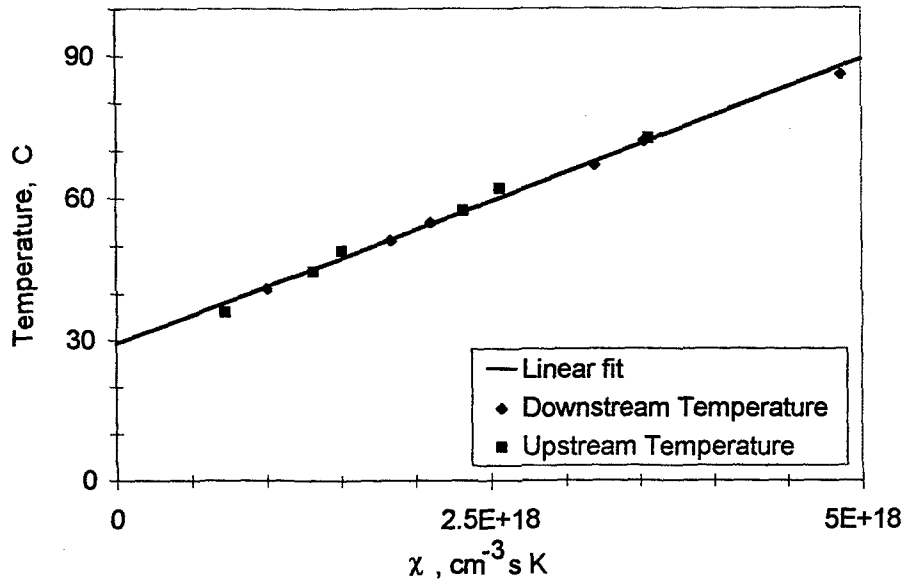

Fig. 6: Downstream and upstream temperatures (degrees Celsius) as a function of modified chi factor. The points represent data extracted from Fig. 5 experimental run for both low and high chlorine flow rate regions. The linear fit slope gives the pooling reaction constant multiplied by the yield squared.

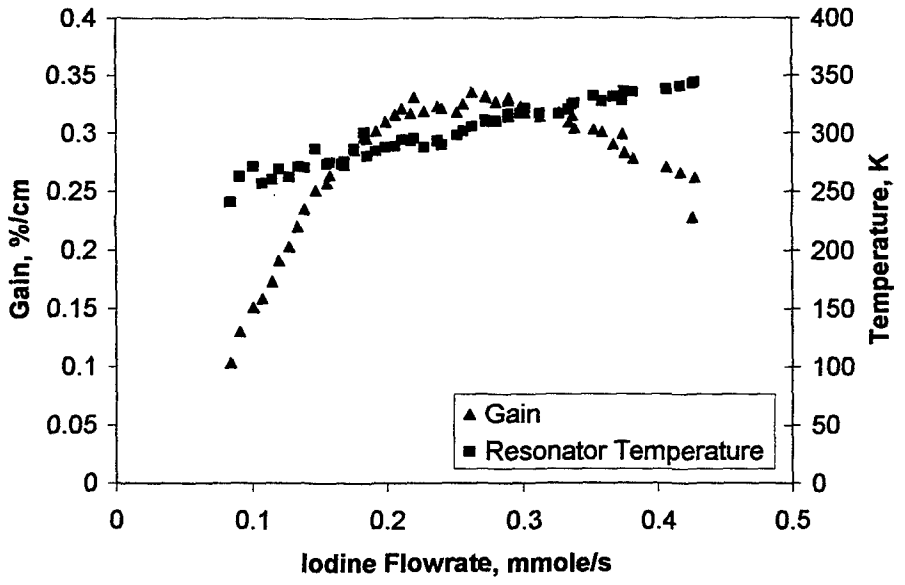

Fig. 7. Gain and temperature at the resonator optical axis as functions of iodine flow rate. Chlorine and secondary nitrogen flow rates are 11.7 and 1.35 mmole/s, respectively, pressures in the generator and resonator are 20 Torr and 1.3 Torr, respectively, and the measured yield is 0.65.

Revised
To be published
in IEEE-JQE (1999)

Diode-laser based absorption spectroscopy diagnostics of a jet-type $O_2(^1\Delta)$ generator for chemical oxygen-iodine lasers

D. Furman, B. D. Barmashenko and S. Rosenwaks

Department of Physics, Ben-Gurion University of the Negev, Beer-Sheva 84105, Israel

ABSTRACT

Using diode laser based diagnostics, $O_2(^1\Delta)$ yield and water vapor fraction were measured at the exit of a jet-type singlet oxygen generator (JSOG), for a chemical oxygen-iodine laser (COIL). Chlorine utilization and gas temperature at the generator exit were also measured, simultaneously. For conditions corresponding to the maximum chemical efficiency of the supersonic COIL energized by the JSOG, the $O_2(^1\Delta)$ yield, water vapor fraction, chlorine utilization and temperature at the generator exit are 0.65, 0.08 and 0.92 and 30 C, respectively. Increase of the basic hydrogen peroxide temperature results in increase of the water vapor fraction caused by increase of the saturated water vapor pressure in the generator. As the pressure in the generator rises from 18 to 60 Torr the yield decreases from 0.65 to 0.48. Dependence of the yield on the generator pressure is consistent with a rate constant of the $O_2(^1\Delta)$ energy pooling reaction of 2.7×10^{-17} cm^3s^{-1}. The same rate constant explains the measured variation of the temperature along the flow in the diagnostic cell.

Keywords: chemical lasers, semiconductor lasers, oxygen, iodine, power lasers.

I. INTRODUCTION

The chemical oxygen-iodine laser (COIL) emits at 1.315 microns on the transition between the spin-orbit levels of the ground state configuration of the iodine atom, $I(5p^5\ ^2P_{1/2}) \rightarrow I(5p^5\ ^2P_{3/2})$ [1] - [3]. The upper level is populated by near-resonant energy transfer from an $O_2(^1\Delta)$ molecule:

$$O_2(^1\Delta) + I(^2P_{3/2}) \rightarrow O_2(^3\Sigma) + I(^2P_{1/2}). \qquad (1)$$

$O_2(^1\Delta)$ is produced in a chemical generator by the reaction of gaseous chlorine with HO_2^- ions which are obtained in a basic hydrogen peroxide solution (BHP). Mixing of $O_2(^1\Delta)$ with I_2 molecules results in their dissociation to iodine atoms which are subsequently excited via reaction (1). $O_2(^1\Delta)$ is deactivated in the volume between the generator exit and mixing point due to the energy pooling reaction

$$O_2(^1\Delta) + O_2(^1\Delta) \rightarrow O_2(^3\Sigma) + O_2(^1\Sigma) \qquad (2)$$

followed by fast quenching of $O_2(^1\Sigma)$ by water:

$$O_2(^1\Sigma) + H_2O \rightarrow O_2(^1\Delta) + H_2O. \qquad (3)$$

As shown in [2] - [5] the laser power strongly depends on the yield of $O_2(^1\Delta)$

$$Y \equiv [O_2(^1\Delta)]/([O_2(^1\Delta)] + [O_2(^3\Sigma)]). \qquad (4)$$

The power also depends on the water vapor fraction in the flow, chlorine utilization and temperature (which rises along the flow due to heat release in reactions (2) and (3)). Generally, the power rises with yield and utilization and falls when the water vapor fraction and temperature increase. To predict the COIL performance and understand the processes in the laser active medium it is important to measure the exact values of the above parameters at

the exit of the $O_2(^1\Delta)$ chemical generator and their dependencies on the flow conditions in the generator.

While the chlorine utilization can be accurately measured using absorption of a probing UV beam [6], it is not as easy to measure yield and water vapor fraction. Usually, $O_2(^1\Delta)$ density is measured by monitoring $O_2(^1\Delta)$ emission at 1.27 μm with a calibrated intrinsic Ge detector [7]. However, this detector is difficult to calibrate and the results exhibit low absolute accuracy in the yield. Another possible method, recently employed in [8], is direct measurement of $O_2(^1\Delta)$ and $O_2(^3\Sigma)$ using spontaneous Raman imaging. Water vapor density was usually evaluated using an indirect method based on a rapid quenching of $O_2(^1\Sigma)$ (formed in reaction (2)) by water molecules (reaction (3)) [9].

Recently, Physical Sciences Inc. [10] developed two diagnostic systems to monitor directly water vapor and ground state oxygen (and hence infer $O_2(^1\Delta)$). Each system is based on sensitive absorption spectroscopy by tunable near infrared and red diode lasers scanning a single rovibrational line of H_2O and a single rotational-electronic line of $O_2(^3\Sigma)$. These diagnostics were used before to measure yield of $O_2(^1\Delta)$ produced by disc type generator in RADICL, a 5 kW class supersonic COIL [11].

In the present paper we report on application of the diode-laser based diagnostics to measure $O_2(^1\Delta)$ yield and water vapor fraction at the exit of jet type, singlet oxygen generator (JSOG) for COIL. In this type of JSOG, first described in [12], the chlorine flow interacts with liquid jets of BHP moving in the opposite direction. High jet velocities (10-20 m/s) reduce depletion of HO_2^- ions at the gas-liquid interface. As a result the JSOG can produce $O_2(^1\Delta)$ with yield greater than 0.5 at high oxygen pressures (up to 30 Torr) in the generator [12]. Today, the jet type generators are widely used in COILs in many laboratories, [13], [14], [15] and is one of the most promising generators of $O_2(^1\Delta)$ for COIL.

In addition to the $O_2(^1\Delta)$ yield and water vapor fraction, the chlorine utilization and gas temperature at the generator exit are measured. All the measurements are done for wide range of the generator pressures, chlorine flow rates and BHP temperatures. Comparison between the experimental data and results predicted by simple model of the JSOG enables us to estimate the rate constant of $O_2(^1\Delta)$ gas phase self-quenching.

II. EXPERIMENTAL SETUP

The experimental setup (Fig. 1) is similar to that used in [16] and [17]. The JSOG {1} used to produce $O_2(^1\Delta)$ is the same as described in [17]. The BHP is prepared from 3 L 50% wt H_2O_2 + 2.5 L 55% wt KOH (6.5 M HO_2^- and 3.3 M H_2O_2 in excess) and kept at -20°C. The jets back pressure [17] is 1.6 atm, which corresponds to BHP flow rate of ~ 0.3 L/s. An exit valve {2} is used to regulate the gas pressure in the JSOG reaction zone. Most of the chlorine reacts with the BHP to produce singlet oxygen. The oxygen flows through the exit to the diagnostic cell {3}, which serves as an interface between the generator and the iodine injector housing. The cell is 14 cm long in the flow direction with a 5 x 1 cm^2 flow cross section. It is equipped with two ports for pressure measurements, two ports for temperature measurements and three interfaces for optical absorption measurements. These identical optical interfaces are used for the chlorine, oxygen and water vapor absorption measurements. The location of the optical axes of the interfaces are 7.5, 11.5 and 15.5 cm downstream of the generator exit, while the temperatures ports are located at 9.5 and 13.5 cm. The iodine-oxygen mixing system {4} is located downstream of the diagnostic cell and is the same as described in [17]. In the present study this system is used in some experimental runs to regulate the choking of the flow (see section IIID), rather than to mix iodine, by varying the secondary nitrogen flow rate. The pumps provide a volumetric flow rate of 450 L/s.

III. MEASUREMENTS AND ERRORS

To find the Cl_2 utilization, the water vapor fraction and the $O_2(^1\Delta)$ yield, one has to measure the following parameters: total pressure, temperature, chlorine density, water vapor density and ground state oxygen density. Below in this section we describe the measurements of these parameters and estimate the errors (all the errors are standard deviations). The water and ground state oxygen are monitored by two special diagnostic systems developed by Physical Sciences Inc. [10] and described below (sections III B and C) in more detail. The chlorine flow rate is controlled and measured by a mass-flow controller (Tylan, model FC-280), limited to a maximum flow rate of 22 mmole/s.

A. Pressure and temperature

The pressure in the generator and in the diagnostic cell is measured as described in [17]. The pressure gauges are routinely checked against a calibrated gauge, which is used solely for this purpose. The pressure gradient in the cell is found to be negligibly small. The accuracy of the pressure measurement is ± 0.1 Torr. The projected error is ± 0.004 in the yield and negligible (compared to other sources of errors) in the water vapor fraction and chlorine utilization.

The temperature sensors, positioned at the center of the flow cross section at the temperature port locations, are glass coated, thin film, platinum resistor probes (RTD devices, RS catalog #237-1607). The area of the gas/sensor interface is 2 mm^2 which is 100 times larger than the cross section of the sensor leads. As shown below (see Fig. 9) the sensor exhibits stable temperature for stable flow conditions, although the diagnostic cell (which is in direct contact with the sensor leads) heats up. That means that only the gas temperature rather than the leads or the wall of the duct affects the sensor. The temperature gradient in the diagnostics cell is large and one needs the temperature at the location of the optical absorption probe in order to calculate partial pressure from density.

The temperature in the cell is assumed to have a constant gradient and is linearly extrapolated from the two locations of temperature measurement to the location of the optical probe. The extrapolated temperature accuracy is estimated to be better than 5 K and the projected error is negligible in the yield, water vapor fraction and utilization.

B. Chlorine partial pressure and utilization

The chlorine utilization in the JSOG is found from the number density of unreacted Cl_2 in the diagnostic cell {3}, the pressure and the temperature. The density of Cl_2 is determined by measuring the absorption at 350 nm. The chlorine density measurement system consists of a stabilized tungsten-halogen lamp, chopper, fiber optics, 350±5 nm filter and a lock-in amplifier in a single beam configuration. Making sure that the signal level is the same at the beginning and end of the experimental run validates the results (if the windows get dirty during the experiment the results are erroneous).

The system was calibrated by measuring the absorption cross section in pure chlorine flow. The measured cross section is within 10% deviation from the value published elsewhere [18]. The main errors in chlorine partial pressure are due to changes of radiation from the stabilized lamp, $\pm 0.5\%$, which corresponds to ± 0.1 Torr, and the accuracy of the pressure gauge (used in the calibration), ± 0.1 Torr. The projected chlorine error in the $O_2(^1\Delta)$ yield is ± 0.008. The main contribution to the error in the utilization comes from the lamp (the total pressure was measured by the same gauge used for the system calibration) so the estimated total error in the utilization is ± 0.01.

C. Water vapor partial pressure and fraction

The water diagnostic is based on a diode laser system which scans an individual rovibrational line of the water $\nu_1 + \nu_3$ band in the 1.39-μm region. The laser beam is split to signal and reference beams. The signal beam is passed through a 5-cm-width diagnostic cell and compared with the reference beam. Under our conditions this system is able to measure water molecule number densities as low as 10^{15} cm^{-3}. The main error in H_2O density measurements is due to the somewhat arbitrary way one sets the profile integration borders in the provided software. Reasonable settings give density deviations of about 5% which corresponds to ± 0.05 Torr. The projected H_2O density error in the $O_2(^1\Delta)$ yield is $\pm$ 0.002. The total error in the water vapor fraction is ± 0.005 (up to ± 0.01 for high water content conditions).

D. Oxygen ground state density

The oxygen diagnostic system measures oxygen ground state ($O_2(^3\Sigma)$) density. It is based on a diode laser that scans an R5R5 line of the $O_2(^3\Sigma) \rightarrow O_2(^1\Sigma)$ electronic-rotational transition. The frequency of the transition measured by the manufacturer of the diagnostic systems (Physical Sciences Inc.) is 13136.206 cm^{-1} (wavelength of 761.2 nm), the accuracy of the measurement being $\pm$ 0.02 cm^{-1} [21]. Like in the water system the laser beam is split to reference and signal. However, since the absorption is very weak, the signal beam is passed 21 times through the 5-cm-width diagnostic cell, in a multi-pass Herriott cell configuration

[22]. The beams are then compared by a balanced ratiometric detector (BRD) which amplifies the logarithm of the ratio between the reference and the signal. The diagnostic is calibrated in the beginning and end of every experimental run by measuring the area under the absorption line for medical-grade oxygen (99.5% minimum) at pressures from 1 to 6 Torr. The calibration curve is always very linear and the offset is smaller than the accuracy of the pressure gauge (0.1 Torr), but the calibration constant (the slope of the curve) can vary up to 10% when comparing the "beginning" and "end" calibrations. The reason for that is the inherent non-linearity of the logarithmic output of the BRD. The optical signal changes during the experiment because of droplets on the windows, and the manufacturer-supplied correction factor is unable to completely correct the non-linearity. In addition, there is a temperature correction factor that comes from the changing gas temperature in the calibration and experimental runs. This factor corrects for the dependence of the absorbing (oxygen ground state) rotational level (j = 5) population on the temperature. The error in the ground state density caused by the change of the signal is up to 10% and is much larger than from other sources, such as absorption line area and temperature. The projected error in the $O_2(^1\Delta)$ yield is about ± 0.035.

E. Yield

The yield of $O_2(^1\Delta)$ is inferred assuming that whatever is not chlorine, water or ground state oxygen, is $O_2(^1\Delta)$:

$$Y = 1 - P_{ox} / (P - P_c - P_w), \qquad (5)$$

where P is static pressure, P_{ox}, P_c and P_w are the partial pressures of ground state oxygen, chlorine and water, respectively. This assumption is justified by the fast quenching of $O_2(^1\Sigma)$ molecules by H_2O (reaction (3), 6.7×10^{-12} cm^3 /s [3]) , the very fast quasi-resonant energy transfer from vibrationally excited $O_2(^3\Sigma, v)$ to H_2O bending vibration ($\sim 10^{-12}$ cm^3/s [19], [20], followed by very fast V-T self-relaxation of H_2O) and the high content of H_2O in the flow (about 10%, see section IVB). Taking into account all the above projected errors, the total

error in the yield is estimated to be about ± 0.05. This value is the sum of the projected errors of each factor in Eq. (5) given in sections III A -D. The main source of error is the change in the level of the oxygen signal beam due to droplets falling on the cell windows, and the non-linearity of the BRD with respect to this signal level. It is possible to reduce this error by making shorter experimental runs or avoiding the droplets in some way.

IV. RESULTS AND DISCUSSION

A. Chlorine utilization

Chlorine utilization vs. residence time of the gas in the generator is plotted in Fig. 2. The residence time is estimated using the known cross section and length of the reaction zone, the measured chlorine flow at the generator inlet, the partial Cl_2+O_2 gas pressure and the gas temperature. The $Cl_2 + O_2$ partial pressure is calculated from the measured gas pressure in the generator (we neglect gas pressure gradient in the generator) and the water fraction in the generator. The water fraction is assumed to be the same as the water fraction in the diagnostic cell (see below in section IV B).

Fig. 2 includes data from many experiments with different chlorine flow rates and generator gas pressures. It is seen that the utilization is usually higher than 0.9 and slowly increases with the residence time. For standard operating conditions corresponding to maximum laser power in experiments [17] (11.7 mmole/s of chlorine, 20 Torr in the generator and residence time of 6 ms) the utilization is 0.92 ± 0.01.

Fig. 3 shows that utilization decreases as the chlorine flow rate increases without changing the generator outlet cross section (the opening of the exit valve). This effect can be explained by the increase of the gas velocity in the generator with chlorine flow rate due to the decrease in boundary layer thickness resulting from the pressure increase. The velocity increase results in a decrease of the gas residence time in the reaction zone, and hence in decrease of the utilization (see Fig. 2).

B. Water vapor

Water vapor density was measured in the diagnostic cell. The water vapor partial pressure in the generator can be calculated assuming that the water vapor fraction in the diagnostic cell is the same as in the generator. Fig. 4 shows the generator total pressure and the partial water vapor pressure in a typical experimental run in which the generator total pressure was changed by adjusting the generator exit valve. The relative change in the water vapor partial pressure is much smaller than the change in the total pressure. In addition, the water vapor pressure tends to stabilize, with time, in some equilibrium pressure. It is concluded that in steady state conditions, the water vapor partial pressure is close to saturation.

Fig. 5 shows the effect of BHP temperature on the partial water vapor pressure in the generator. As the BHP bulk temperature was allowed to rise with time (simply by turning off the cooling), the water vapor pressure in the generator increased. Comparison between these results and theoretical temperature dependence of saturated water vapor pressure above BHP (presented in [23]), shows that the "effective" temperature of the jet surface is six to seven degrees higher than the measured bulk temperature. The temperature of the jets is expected to be higher than the bulk temperature because of heat exchange in the gear pump and transport line, and because of the jet surface reactions.

Fig. 6 summarizes the results of many experimental runs. The water vapor fraction in the flow is plotted against the generator total pressure for BHP temperature between –16°C to -18°C (the partial water vapor weakly depends on the temperature in this range). The accuracy of measurement of each experimental point is much better than the scattering of the points in the graph (see section III C). The explanation for the scattering is that during many experiments it was possible to see, in the diagnostic cell, some amount of liquid being carried out by the flowing gas out of the generator. In that instant the water vapor density (and fraction) was noticed to rise considerably. For standard operating conditions (see section IV A) and a dry diagnostic cell, the water vapor fraction was 0.08 ± 0.01.

C. Yield

The yield is plotted in Fig. 7 as a function of the generator Cl_2 + O_2 partial pressure, which was found as described in section IV A. In some experiments the ground state oxygen diagnostic was positioned 4 cm upstream of the center of the diagnostic cell, in the others 4 cm downstream. There is not much difference between these two sets of results. This is in agreement with energy loss computations (Chi analysis [24]) that take into account the pooling reaction (2). The figure shows also two calculated curves which were obtained using a surface chemistry model (referred to also as "well stirred limit" model) [25] where depletion of HO_2^- ions near the gas-liquid interface is neglected and only gas-phase losses of $O_2(^1\Delta)$ in the pooling reaction (2) are taken into account. The model, described in more detail in Appendix A, has two fitting parameters: the chlorine lifetime in the JSOG, τ, and detachment yield, Y_0. The values of τ and Y_0 were chosen to fit the measured utilization and yield at Cl_2 + O_2 partial pressure of 18 Torr (corresponding to the flow static pressure of 20 Torr). Pressure dependencies of Y are calculated for two different values of the rate constant k_p of $O_2(^1\Delta)$ deactivation. The first value, 2.7 x 10^{-17} cm^3/s [26], is the rate constant of reaction (2), whereas the second value, 6.1 x 10^{-17} cm^3/s [27], is the effective rate constant of $O_2(^1\Delta)$ deactivation taking into account both reaction (1) and the reaction $O_2(^1\Delta) + O_2(^1\Delta) \rightarrow 2O_2(^3\Sigma)$. It is seen that using the lower rate 2.7 x 10^{-17} cm^3/s in the calculations gives a better agreement with experimental results. The yield measured for standard operating conditions (see section IV A) is 0.65 ± 0.05.

Fig. 8 shows how the yield increases when the chlorine flow rate is increased without changing the generator outlet cross section. The yield increases as a result of lower pooling losses, as the decrease in gas residence time (see discussion of Fig. 3 in section IV A) more than compensates for the increase in oxygen density.

D. Temperature

Fig. 9 shows the behavior of the temperature measured in two points along the flow (see section III A). Until the 200th second the diagnostic cell pressure was changed (at the 40th, 80th, 125th seconds) without changing Cl_2 flow rate. This was achieved by injecting N_2

downstream of the diagnostic cell (through the iodine-oxygen mixing system {4}) and choking the flow. It is seen that the temperature and the temperature difference increase in the diagnostic cell with the cell pressure. After the 200th second, when we increased the chlorine flow rate, there was a minor increase in temperature. At the 260th second we increased the cell pressure again.

Neglecting heat transfer from the gas to the walls of the diagnostic cell and the change of the yield Y along the flow in the cell (see discussion of Fig. 7), the gas temperature is given by

$$T = T_i + \chi_T k_P Y^2, \qquad (6)$$

where T_i is the temperature at the generator exit,

$$\chi_T = \frac{q_\Delta}{c_P}\left(\frac{p}{kT_{AV}}\right)^2 \frac{n_{O2}{}^2 V}{n^3} \qquad (7)$$

is a modified "chi" factor (definition of the usual "chi" factor is given in [24]), q_Δ is the energy of $O_2(^1\Delta)$, $c_P = 7/2$ k is the heat capacity of a diatomic gas, $T_{AV} = 0.5(T+T_i)$ is the average temperature, n_{O2} and n are the oxygen and total flow rates, respectively, and V is the volume over which the losses are calculated. Eq. (6) is valid only if the densities of $O_2(^1\Sigma)$ and vibrationally excited $O_2(^3\Sigma)$ and $O_2(^1\Delta)$ are negligibly small. As shown in section III D, for our conditions this assumption is correct.

Fitting a linear graph to the plot of temperatures as a function of the modified chi factor, with T_i equal T as a first iteration, gives the slope $k_P Y^2$ and a better value of T_i. Fig. 10 shows the result after several iterations, when both of the values T_i and $k_P Y^2$ converged. The points are plotted for different flow rates and temperature measurement positions using the appropriate values of volume (from the generator exit to the measuring position) and flow rate. The slope (after several iterations of T_i) is 1.2×10^{-17} cm^3 s^{-1} °C. Using the measured value of the yield (it changes little with flow rate, see Fig. 8), 0.65 ± 0.05, we get $O_2(^1\Delta)$ deactivation rate of $(2.8 \pm 0.5)\cdot 10^{-17}$ cm^3 s^{-1}. This value is in agreement with a pooling

reaction rate constant $k_p = 2.7 \times 10^{-17}$ cm^3/s rather than with the effective rate constant $k_p = 6.1 \times 10^{-17}$ cm^3/s (see discussion in section IV C). The agreement remains good if we take into account the temperature dependence of the pooling rate constant [26], [28]

$$kp = 9.5 \times 10^{-28} T^{-3.8} \exp(700/T) \qquad (8)$$

For the average temperature of 330 K Eq. (8) yields $kp = 2.9 \times 10^{-17}$ cm^3 s^{-1} which is close to $(2.8 \pm 0.5) \cdot 10^{-17}$ cm^3 s^{-1}. Effects of heat transfer are estimated to be negligibly small.

Fig. 11 shows the results of another experiment where the generator pressure was increased (without changing the flow) by changing the generator outlet cross section. The gas residence time and density increase with the pressure, causing higher $O_2(^1\Delta)$ losses in the generator, which, in turn, raised the temperature of the gas exiting the generator into the diagnostic cell. The decrease in yield causes a decrease of temperature difference between the downstream and upstream measurement positions. Extrapolated temperature at the generator exit is also shown in Fig. 11. The exit gas temperature for standard conditions is about 30 C and increases as the generator pressure increases. The temperature is much higher than the BHP temperature. From the modified chi analysis we estimate that about half of this difference is due to heat release caused by $O_2(^1\Delta)$ deactivation in the generator in the volume between the BHP jets and the generator exit valve. The other half is due to heat release in the volume occupied by the jets, which may mean that the gas in the generator is not in thermal equilibrium with the BHP jets (contrary to the assumption made in [13], [29]).

We applied the modified chi analysis for the volume and temperature difference between the upstream and downstream temperature measurement positions in order to determine the yield as a function of the generator $O_2 + Cl_2$ pressure. Fig. 12 shows the yield for two reaction rates, together with the measured yield (which was already presented in Fig. 8). The smaller reaction rate of 2.7×10^{-17} cm^3/s makes these sets of measurements (temperature and yield) much more consistent.

V. CONCLUSIONS

Using diode-laser based absorption spectroscopy diagnostics we measured the $O_2(^1\Delta)$ yield and water vapor fraction at the exit of a jet type $O_2(^1\Delta)$ generator for COILs. In addition, the chlorine utilization and gas temperature at the generator exit were measured. All the measurements were done for wide range of generator pressures, chlorine flow rates and BHP temperatures.

For conditions corresponding to the maximum chemical efficiency of the supersonic COIL [17] (12 mmole/s of chlorine, 20 Torr in the generator and BHP temperature of -17 C) the yield, water vapor fraction and utilization are 0.65, 0.08 and 0.92, respectively. The gas temperature at the generator exit is about 30 C. The absolute error of the yield measurements is estimated to be $\pm$ 0.05.

As the pressure in the generator increases (for constant chlorine flow rate) the yield and water vapor fraction decrease, whereas the chlorine utilization and gas temperature at the generator exit increase. When the Cl_2 + O_2 partial pressure increases from 18 to 60 Torr the yield decreases from 0.65 to 0.48, i. e. the decrease of the yield is not large. The dependence of the yield on the generator pressure is consistent with rate constant of the pooling reaction (2) of 2.7×10^{-17} cm^3s^{-1} [26]. The same rate constant explains the measured variation of the temperature along the flow in the diagnostic cell.

Increase of the chlorine flow rate (for constant opening of the generator exit valve) results in a weak increase of the yield and decrease of the chlorine utilization. The generator efficiency, defined as the product of the yield and utilization, is almost independent of the chlorine flow in this range.

Increasing the BHP temperature results in an increase of the water vapor fraction caused by an increase of the saturated water vapor pressure in the generator, the yield and utilization being independent of the temperature.

The parameters of the JSOG exit found here are very useful for parametric studies related to high power COILs and for predicting the output power and gain.

ACKNOWLEDGMENTS

We thank the USAF European Office of Aerospace R&D for equipment grant.

APPENDIX A. SURFACE CHEMISTRY MODEL OF JSOG (WELL-STIRRED LIMIT)

This model, presented in [25], assumes negligibly small depletion of HO_2^- ions near the gas-liquid interface and takes into account only gas-phase losses of $O_2(^1\Delta)$ in the pooling reaction (2). The chlorine utilization η is given by

$$\eta = 1 - \exp(- t_{res}/\tau), \tag{A1}$$

where $t_{res} = l_{gen}/U_g$ is the gas residence time in the JSOG reaction zone and τ is the chlorine lifetime in the JSOG. The change of $[O_2(^1\Delta)]$ is given by

$$d[O_2(^1\Delta)]/dt = (Y_0[Cl_2]_0/\tau)\exp(-t/\tau) - k_p[O_2(^1\Delta)]^2, \tag{A2}$$

where $t = x/U_g$, Y_0 is detachment yield and $[Cl_2]_0$ is initial number density of Cl_2. Approximate solution of Eq. (A2) is given by [25]

$$1/Y=1/Y_0 + f(\eta)\, k_p[O_2(^1\Delta)]\, t_{res}, \tag{A3}$$

where

$$f(\eta) = 1/\eta^2 + (1 + \eta/2) / [\, \eta \ln(1 - \eta)]$$

REFERENCES

[1] W. E. McDermott, N. R. Pchelkin, D. J. Benard, R. R. Bousek, "An electronic transition chemical laser," *Appl. Phys. Lett.*, vol. 32, pp. 469-470, 1978.

[2] K. A. Truesdell and S. E. Lamberson, "Phillips laboratory COIL technology overview," *SPIE*, vol.1810, pp. 476 - 492, 1992.

[3] N. N. Yuryshev, "Chemically pumped oxygen-iodine laser," *Quantum Electronics*, vol.23, pp. 583 - 600, 1996.

[4] B. D. Barmashenko, A. Elior, E. Lebiush and S. Rosenwaks, "Modeling of mixing in chemical oxygen-iodine lasers: Analytic and numerical solutions and comparison with experiments," *J. Appl. Phys.*, vol. 75, pp. 7653-7655, 1994.

[5] J. Hon, D. N. Plummer, P. G. Crowell, J. Erkkila, G. D. Hager, C. Helms and K. Truesdell, "Heuristic method for evaluating Coil performance", *AIAA J.*, vol. 34, pp. 1595-1603, 1996.

[6] W. J. Thayer III and C. H. Fisher, "Comparison of predicted and measured output from a transverse flow uniform droplet singlet oxygen generator" in *25th AIAA Plasmadynamics and Lasers Conf.*, Colorado Springs, CO, June 20-23, 1994, paper 94-2454.

[7] A. Elior, B. D. Barmashenko, E. Lebiush, and S. Rosenwaks, "Experiment and modeling of a small-scale, supersonic chemical oxygen-iodine laser," *Appl. Phys. B*, vol. 61, pp. 37 - 47, 1995.

[8] V. T. Gylys and L. F. Rubin, "Direct measurement of $O_2(a^1\Delta)$ and $O_2(X^3\Sigma)$ in chemical oxygen-iodine lasers with use of spontaneous Raman imaging," *Appl. Opt.*, vol. 37, pp. 1026-1031, 1998.

[9] O. Spalek, J. Kodymova, M. V. Zagidullin and V. D. Nikolaev, "Optimization of jet singlet oxygen generator for chemical oxygen-iodine laser," *SPIE*, vol. 3092, pp.565-568, 1997.

[10] M. G. Allen, K. L. Carleton, S. J. Davis, W. J. Kessler and K. R. McManus, "Diode laser-based messurements of Water vapor and ground state oxygen in chemical oxygen iodine lasers," in *25th AIAA Plasmadynamics and Lasers Conf.*, Colorado Springs, CO, June 20-23, 1994, paper 94-2433.

[11] K. A. Truesdell, C. A. Helms, S. Frerking and G. D. Hager, "COIL performance modeling and recent advances in diagnostic measurements," *SPIE*, vol. 3092, pp.676-681, 1997.

[12] M. V. Zagidullin, A. Y. Kurov, N. L. Kupriyanov, V. D. Nikolaev, M. I. Svistun and N. Y. Erasov, "Highly efficient jet $O_2(^1\Delta)$ generator," *Sov. J. Quantum Electron.*, vol.21, pp. 747-753, 1991.

[13] I. Blayvas, B. D. Barmashenko, D. Furman, S. Rosenwaks, and M.V. Zagidullin, "Power optimization of small-scale chemical oxygen-iodine laser," *IEEE J. Quantum Electronics*, vol. 32, pp. 2051-2057, 1996.

[14] W. E. McDermott, J. C. Stephens, J. Vetrovec and R. A. Dickerson, "Operating experience with a high throughput jet generator," in *28th AIAA Plasmadynamics and Lasers Conf.*, Atlanta, GA, June 23-25, 1997, paper 97-2385.

[15] M. Endo, S. Nagamoto, S. Takeda, M. V. Zagidullin, V. D. Nikolaev, H. Fujii, F. Wani, D. Sugimoto, K. Sunako, K. Nanri and T. Fujioka, "High-efficiency operation of chemical oxygen-iodine laser using nitrogen as buffer gas," *IEEE J. Quantum Electronics*, vol. 34, pp. 393-398, 1998.

[16] D. Furman, B. D. Barmashenko and S. Rosenwaks, "An efficient supersonic chemical oxygen-iodine laser operating without buffer gas and with simple nozzle geometry," *Appl. Phys. Lett.*, vol. 70, pp. 2341-2343, 1997.

[17] D. Furman, B. D. Barmashenko and S. Rosenwaks, "Parametric study of an efficient supersonic chemical oxygen-iodine laser/jet generator system operating without buffer gas," *IEEE J. Quantum Electronics*, vol. 34, pp. 1068 -1074, 1998.

[18] H. Okabe, *Photochemistry of Small Molecules*. New York:Wiley, 1978.

[19] R. L. Taylor and S. Bitterman, "Survey of vibrational relaxation data for processes important in the CO_2-N_2 laser systems," Rev. Mod. Physics, vol. 41, pp. 26 - 47, 1969.

[20] J. D. Lambert, *Vibrational and Rotational Relaxation in Gases.* Oxford: Clarendon Press, 1977.

[21] S. J. Davis and W. J. Kessler , private communication.

[22] H. J. Baker, "Multifold resonators," in *The Physics and Technology of Laser Resonators*, Ed. by D. R. Hall and P. E. Jackson, Bristol: Inst. of Physics, 1992.

[23] M. V. Zagidullin, V. I. Igoshin, V. A. Katulin and N. L. Kupriyanov, "Possibility of operation of a chemical oxygen-iodine laser without a cooled trap," *Sov. J. Quantum Electron.*, vol.13, pp. 75 - 76, 1983.

[24] T. L. Rittenhouse, S. P. Phipps, C. A. Helms and K. A. Truesdell, "High efficiency operation of a 5-cm gain length supersonic chemical oxygen-iodine laser," *SPIE*, vol. 2702, pp.333 - 338, 1996.

[25] D. A. Copeland, W. E. McDermott, V. Quan and A. H. Bauer, "Exact and approximate solutions of the utilization and yield equations for $O_2(^1\Delta)$ generators," in *24th AIAA Plasmadynamics and Lasers Conf.*, Orlando, FL, July 6 - 9, 1993, paper 93-3220.

[26] H. V. Lilenfeld, P. A. G. Carr and F. E. Hovis, "Energy pooling reactions in the oxygen-iodine system," *J. Chem. Phys.*, vol.81, pp. 5730 - 5736, 1984.

[27] G. P. Perram and G. D. Hager, "The standard chemical oxygen-iodine laser kinetics package," U.S. Air Force Weapons Lab., AFWL-TR-88-50, Kirtland AFB, NM, Oct. 1988.

[28] R. F. Heidner III, C. E. Gardner, T. M. El-Sayed, G. E. Segal and J. V. V. Kasper, "Temperature dependence of $O_2(^1\Delta) + O_2(^1\Delta)$ and $I(^2P_{1/2}) + O_2(^1\Delta)$ energy pooling," *J. Chem. Phys.*, vol.74, pp. 5618 - 5626, 1981.

[29] M. V. Zagidullin and V. D. Nikolaev, "Gain saturation and the efficiency of energy conversion into radiation in a supersonic oxygen - iodine laser with a stable cavity,"

Quantum Electron., vol. 27, pp. 411-416, 1997.

FIGURE CAPTIONS

Fig. 1: The experimental setup. (1) jet type singlet oxygen generator, (2) exit valve, (3) diagnostic cell, (4) iodine mixing system (supersonic grid nozzle).

Fig. 2: Chlorine utilization vs. residence time for different chlorine flow rates (10 to 20 mmole/s) and generator gas pressures (15 to 80 Torr).

Fig. 3: Chlorine utilization in the generator vs. chlorine flow rate for constant outlet cross-section. The residence time (hence the utilization) increases when flow rate decreases because of boundary layers effects.

Fig. 4: Gas and water vapor pressures in the generator as a function of time. The data is of a typical experimental run with chlorine flow rate of ~10 mmole/s. The generator gas pressure was changed by changing the generator outlet cross section.

Fig. 5: BHP temperature and water vapor pressure in the generator as a function of time. The data is from a single experimental run with chlorine flow rate of ~10 mmole/s. The BHP temperature starts to decrease when the cooling is turned off.

Fig. 6: Water vapor fraction vs. generator gas pressure for chlorine flow rates between 10 and 12 mmole/s. The graph includes data from experimental runs where liquid droplets where carried out into the diagnostics duct.

Fig. 7: Yield vs. generator gas pressure for two different positions of the oxygen diagnostics (upstream and downstream) and chlorine flow rate of 12 mmole/s. The lines represent calculations of surface reaction model with two different energy pooling reaction rates. The detachment yield Y_0 and the chlorine lifetime where set so the calculations will match the measurements at ~18 Torr.

Fig. 8: Yield vs. chlorine flow rate in two experimental runs with different, constant generator outlet cross section during each run. The upper trace is for low generator pressure (e. g. 18 Torr at 12 mmole/s), the lower trace is for high generator pressure (e. g. 24 Torr at 12 mmole/s). The residence time decreases when the flow rate increases (hence the increase of the yield) because of boundary layers effects.

Fig. 9: Upstream and downstream temperatures (degrees Celsius) in a typical experimental run. The diagnostics cell pressure was manually changed by choking the flow

downstream of the cell. At the 200th second the chlorine flow rate (hence the cell pressure) was increased, note that the temperature was not significantly increased.

Fig. 10: Downstream and upstream temperatures (degrees Celsius) as a function of modified chi factor. The points represent data extracted from Fig. 9 experimental run for both low and high chlorine flow rate regions. The linear fit slope gives the pooling reaction constant multiplied by the yield squared.

Fig. 11: Upstream, downstream and generator exit temperatures as a function of the generator pressure for a constant chlorine flow rate. The generator exit temperature was linearly extrapolated from the upstream and downstream temperatures using the known distances of the temperature sensors from the generator exit. The leftmost set of points was acquired for lower diagnostics cell pressure (hence the lower diagnostics cell temperature).

Fig. 12: Measured yield (Fig. 7) plotted together with yield calculated from the temperature differences between upstream and downstream temperatures. The temperature data is the same as in Fig. 11. The yield was calculated using modified chi analysis, using the known volume between the upstream and downstream temperature measurement locations, for two different pooling reaction rates. It is clear that the smaller reaction rate gives a better consistency between the temperature measurements and the yield measurements.

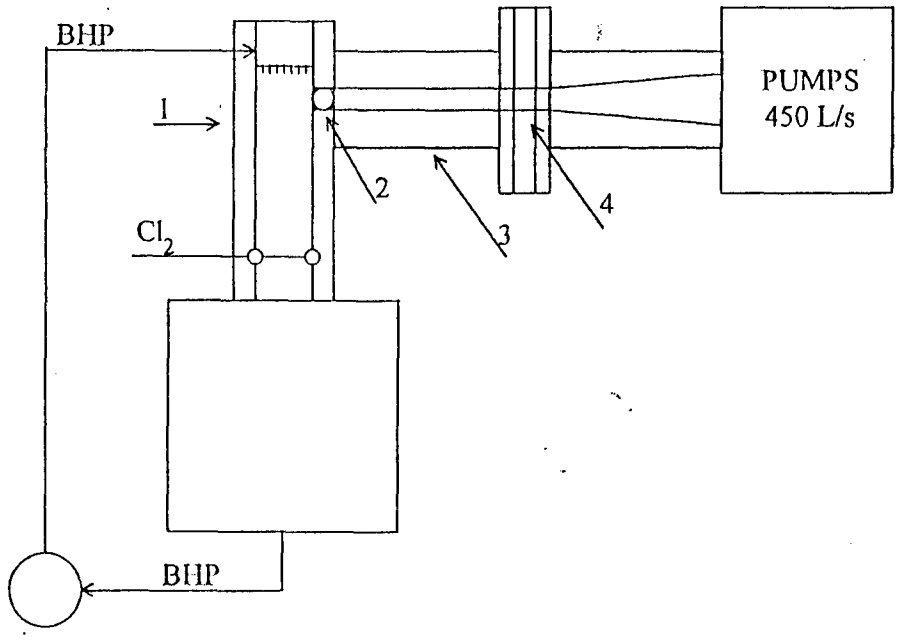

Fig. 1. D..Furman et al. IEEE JQE

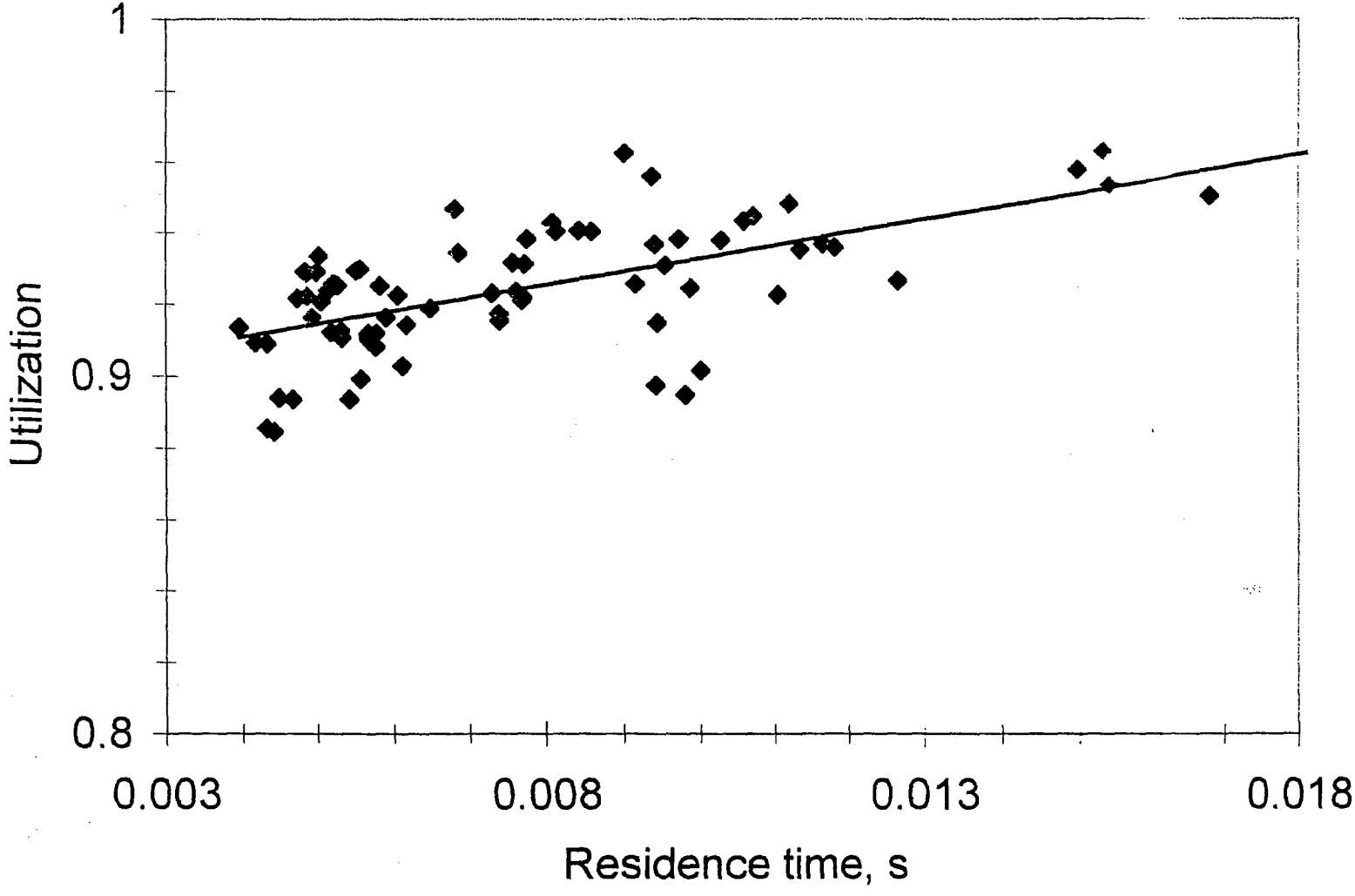

Fig. 2. D. Furman et al. IEEE JQE

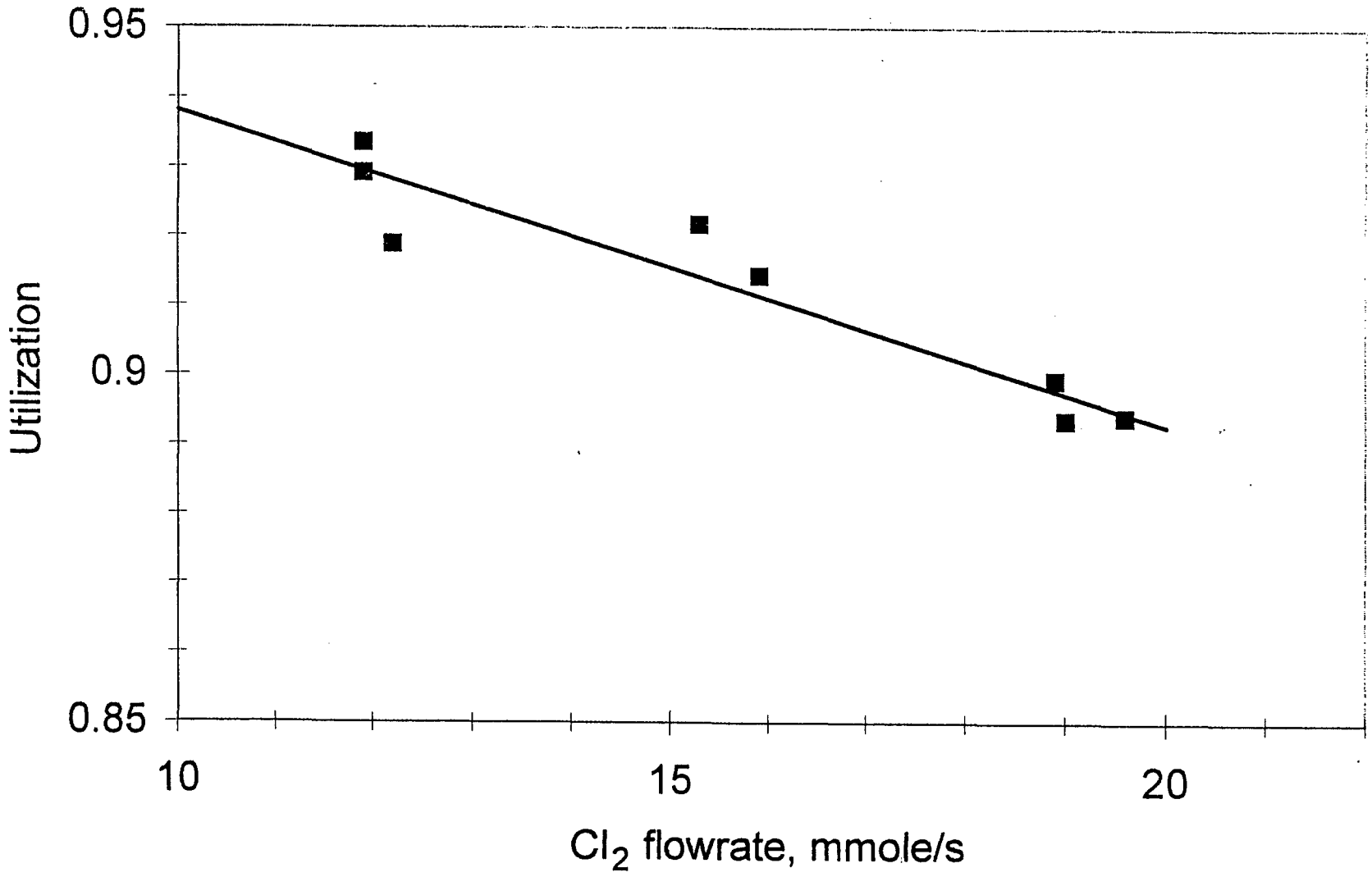

Fig. 3. D. Furman et al. IEEE JQE

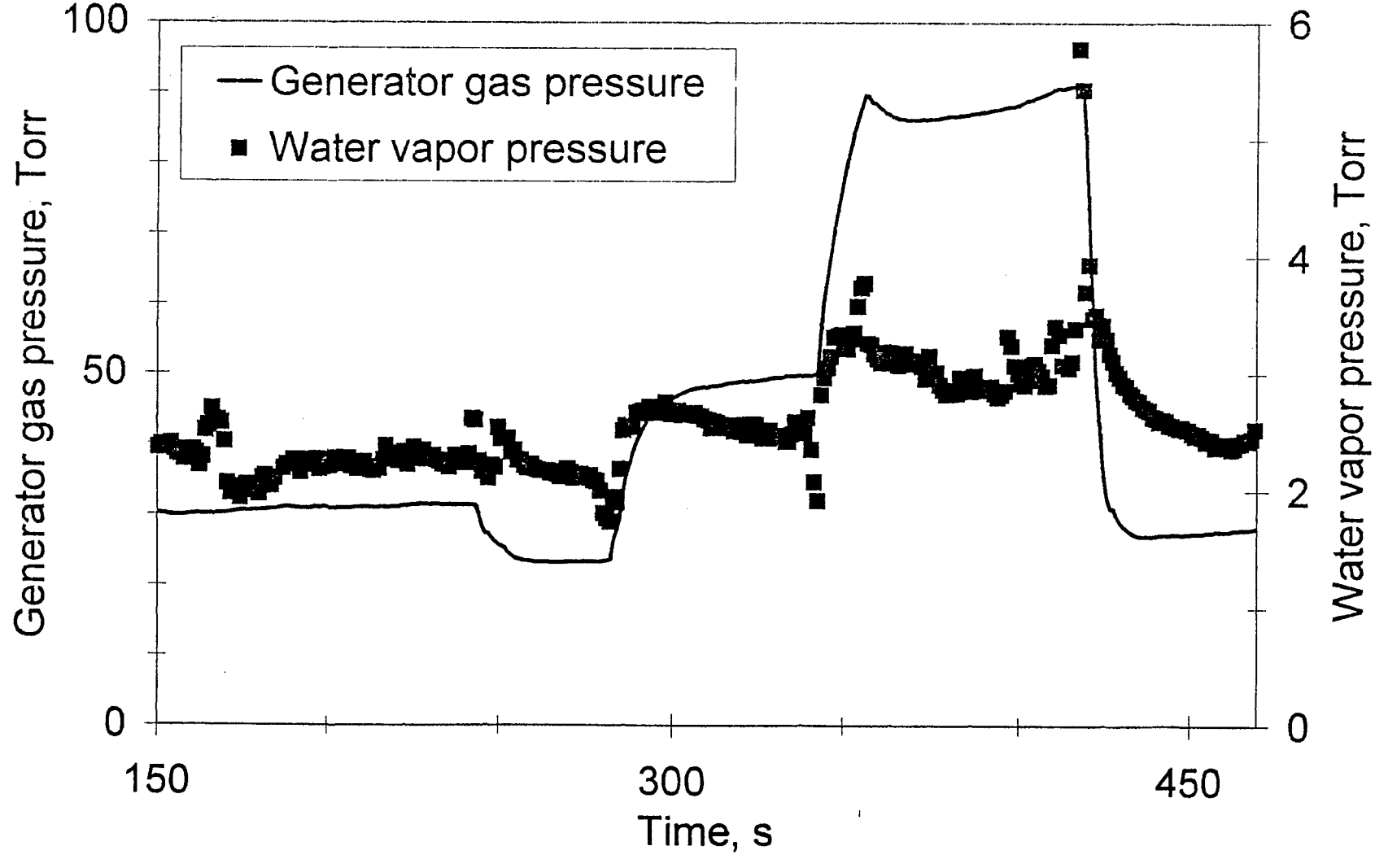

Fig. 4. D. Furman et al. IEEE JQE

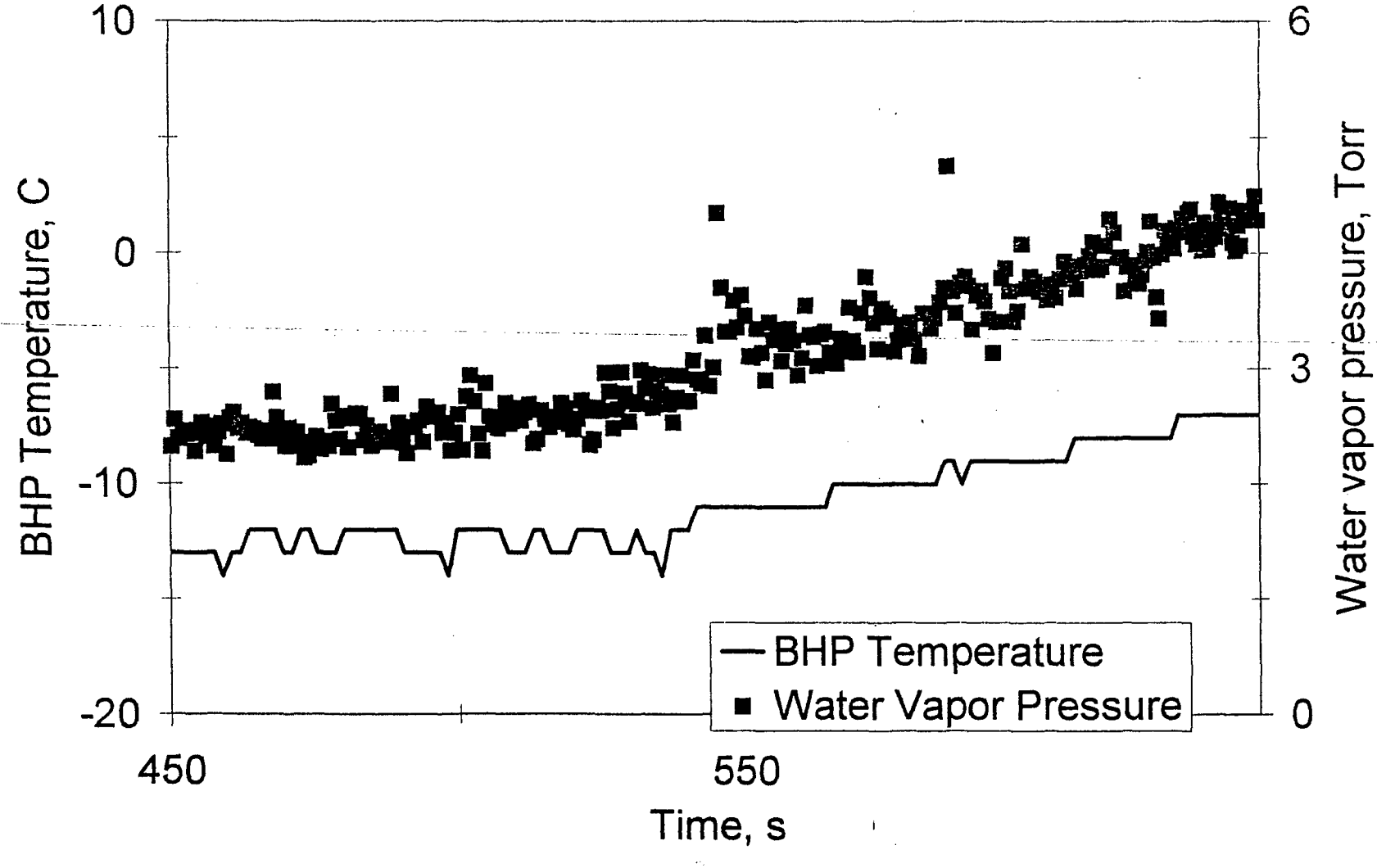

Fig. 5. D. Furman et al. IEEE JQE

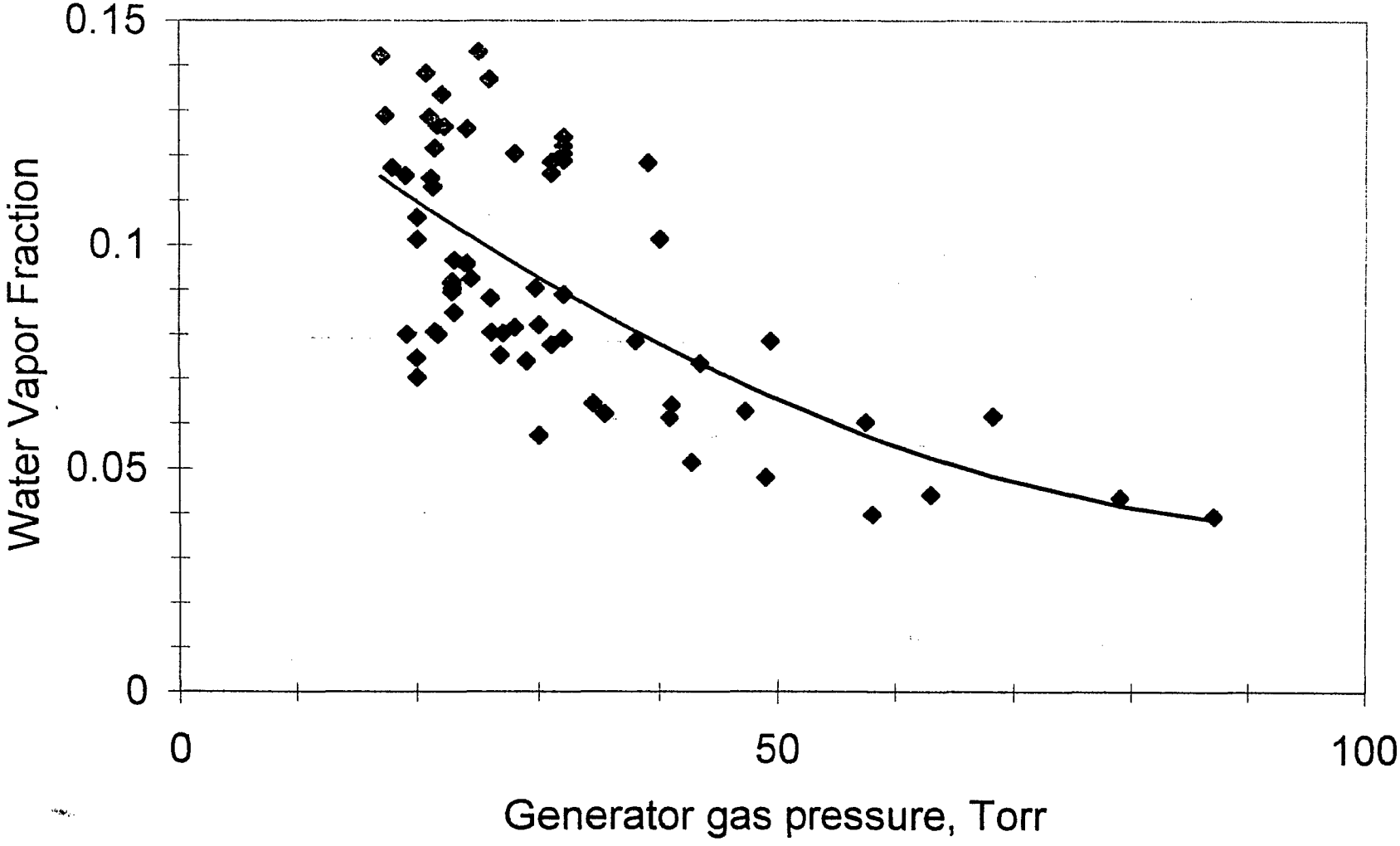

Fig. 6. D. Furman et al. IEEE JQE

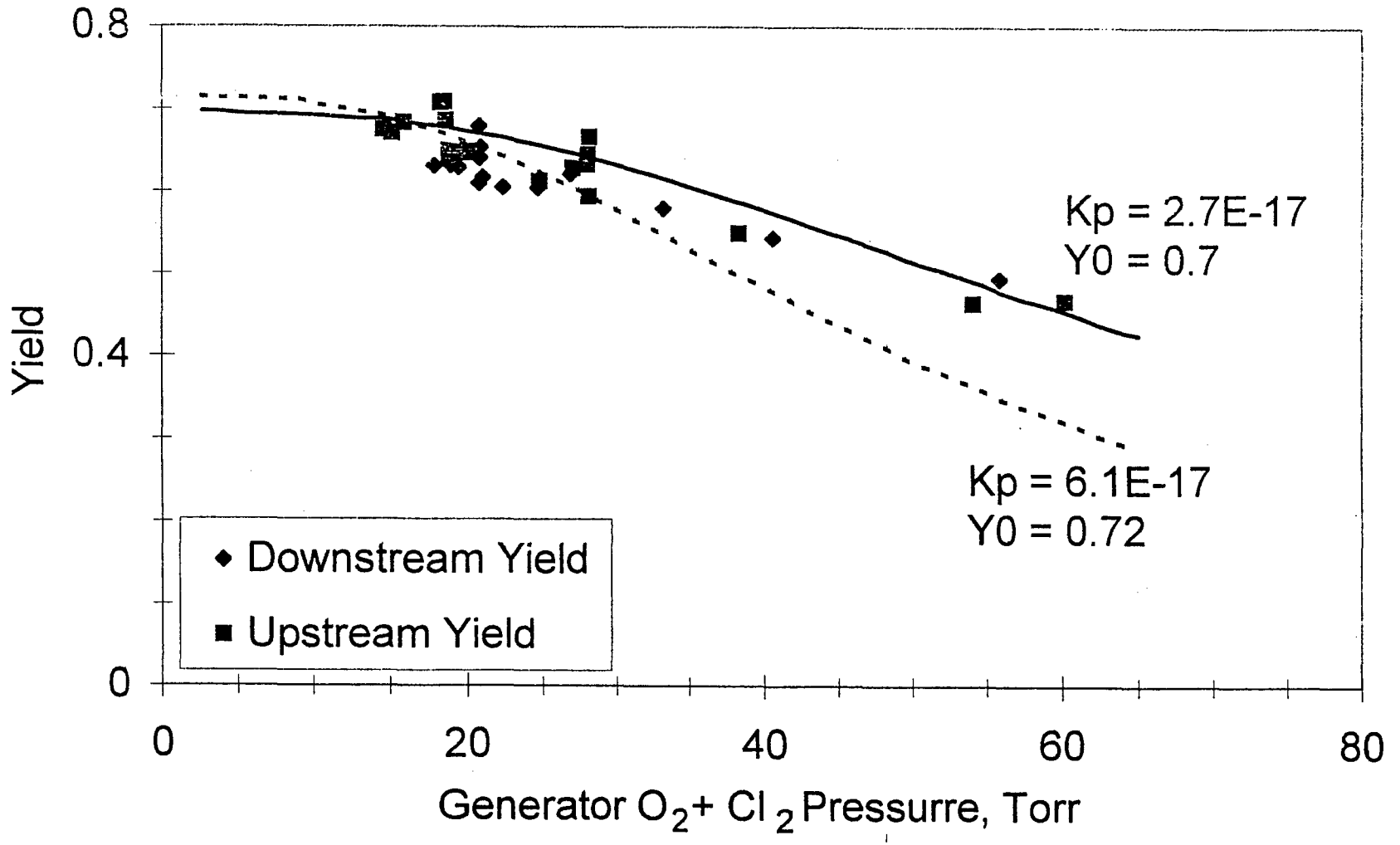

Fig. 7. D. Furman et al. IEEE JQE

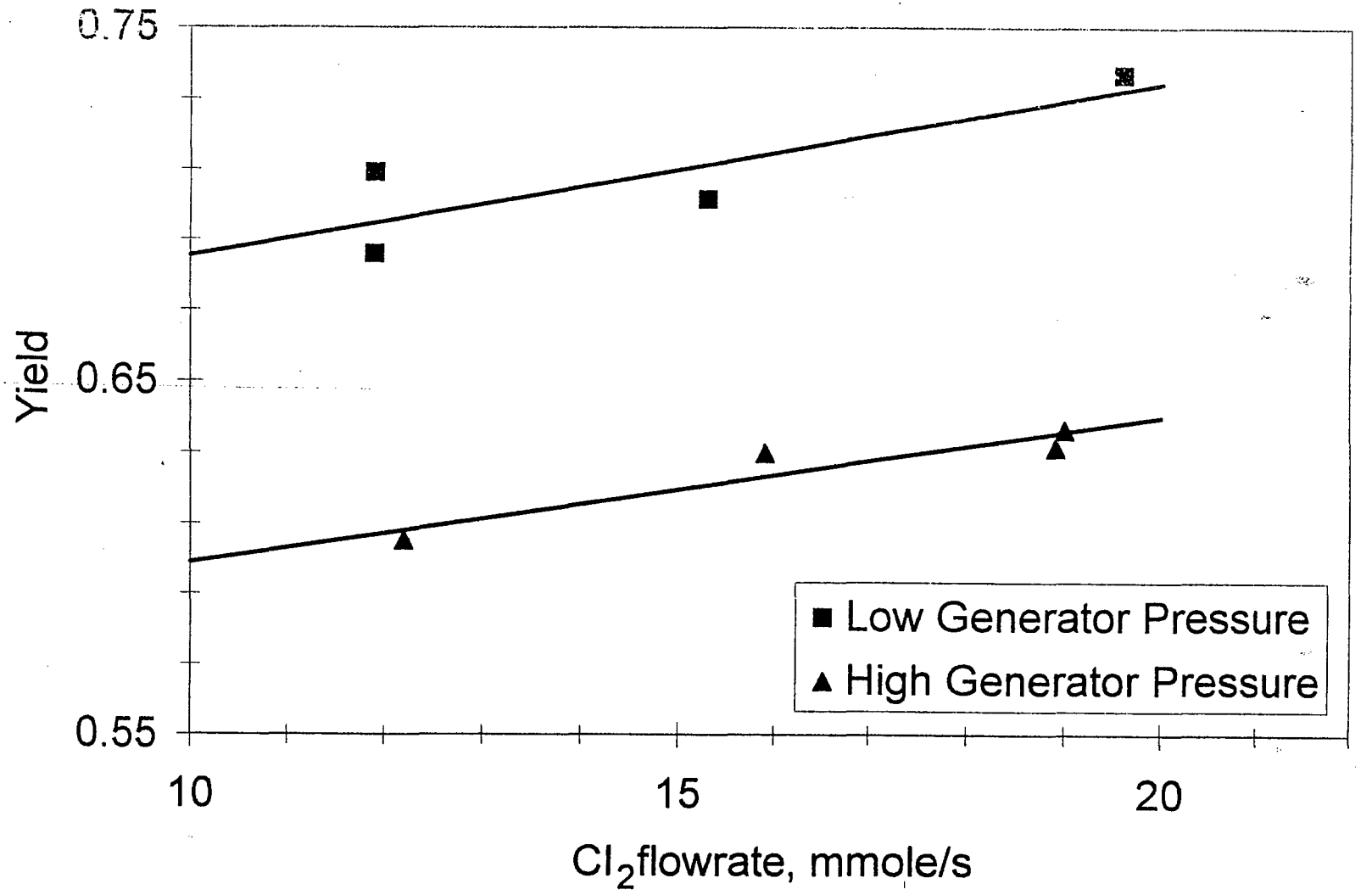

Fig. 8. D. Furman et al. IEEE JQE

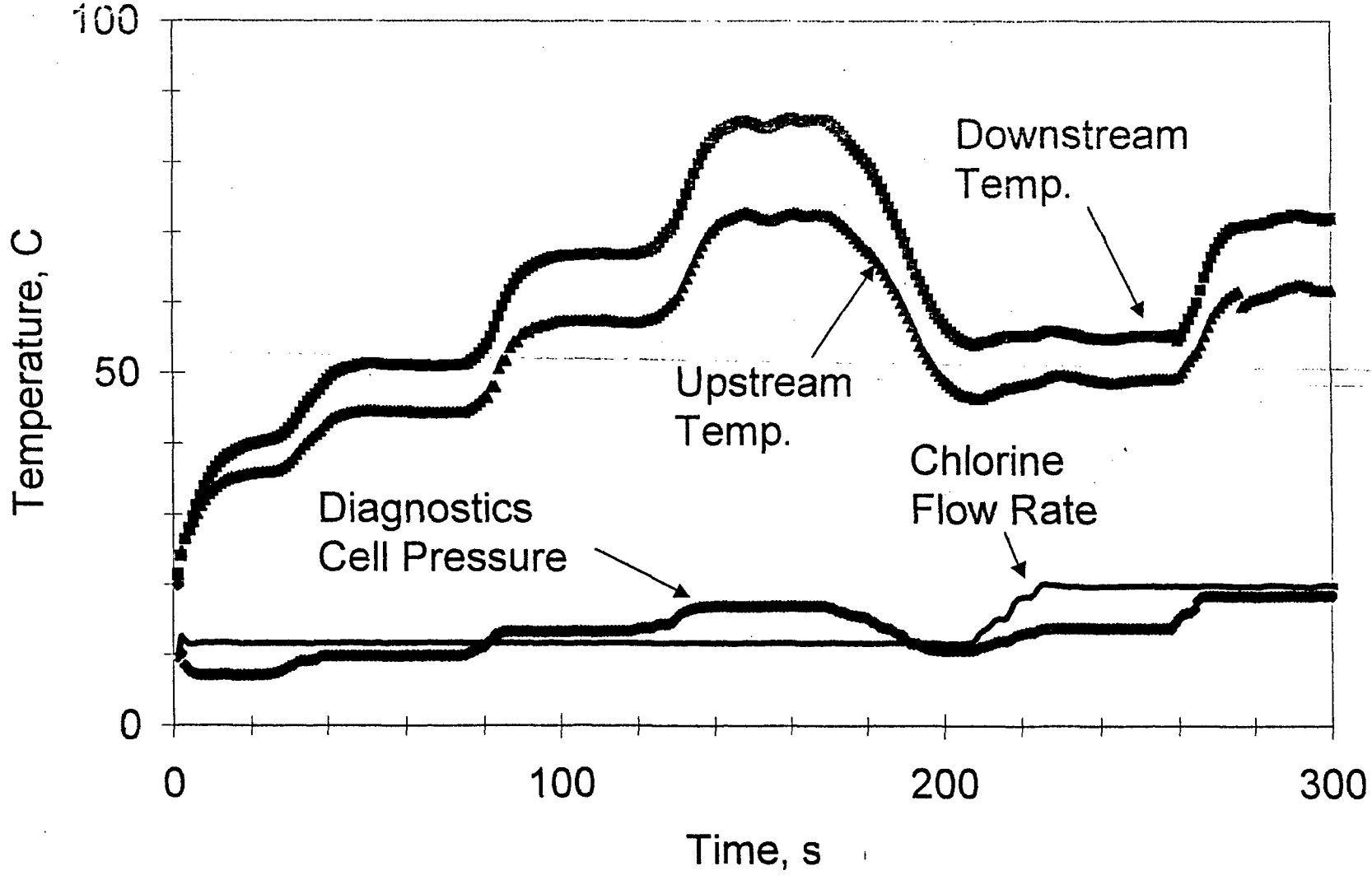

Fig. 9. D. Furman et al. IEEE JQE

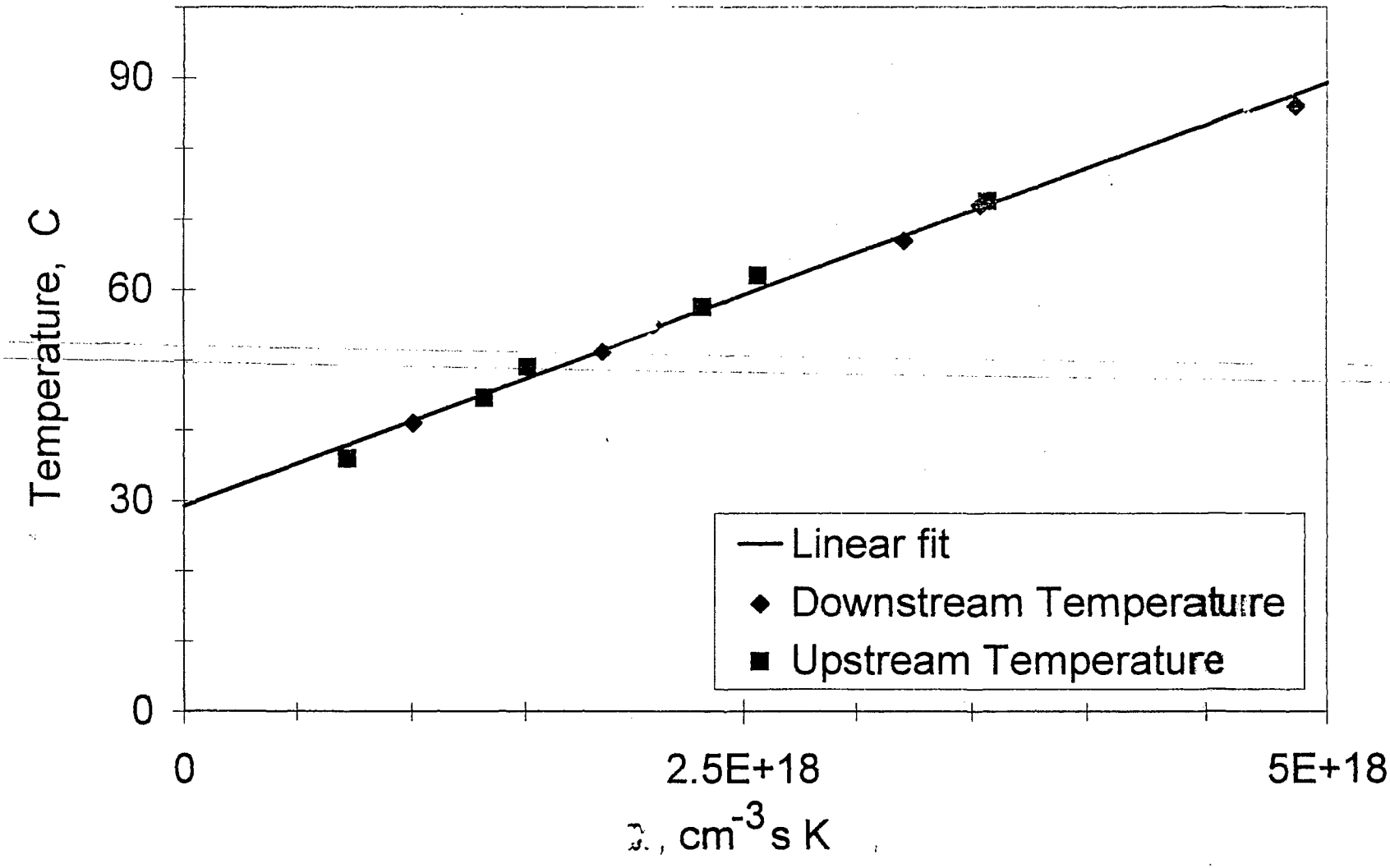

Fig. 10. D. Furman et al. IEEE JQE

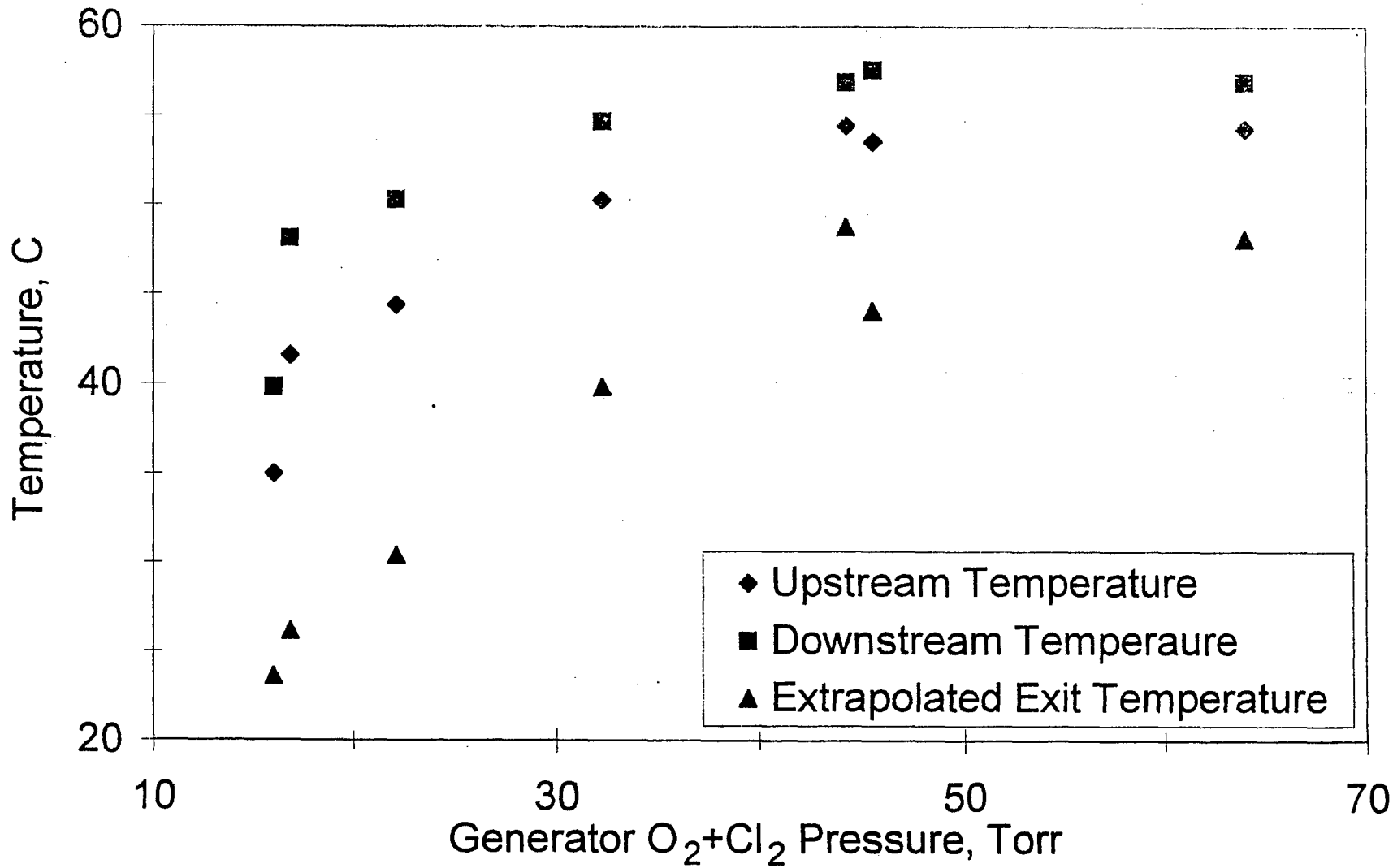

Fig. 11. D. Furman et al. IEEE JQE

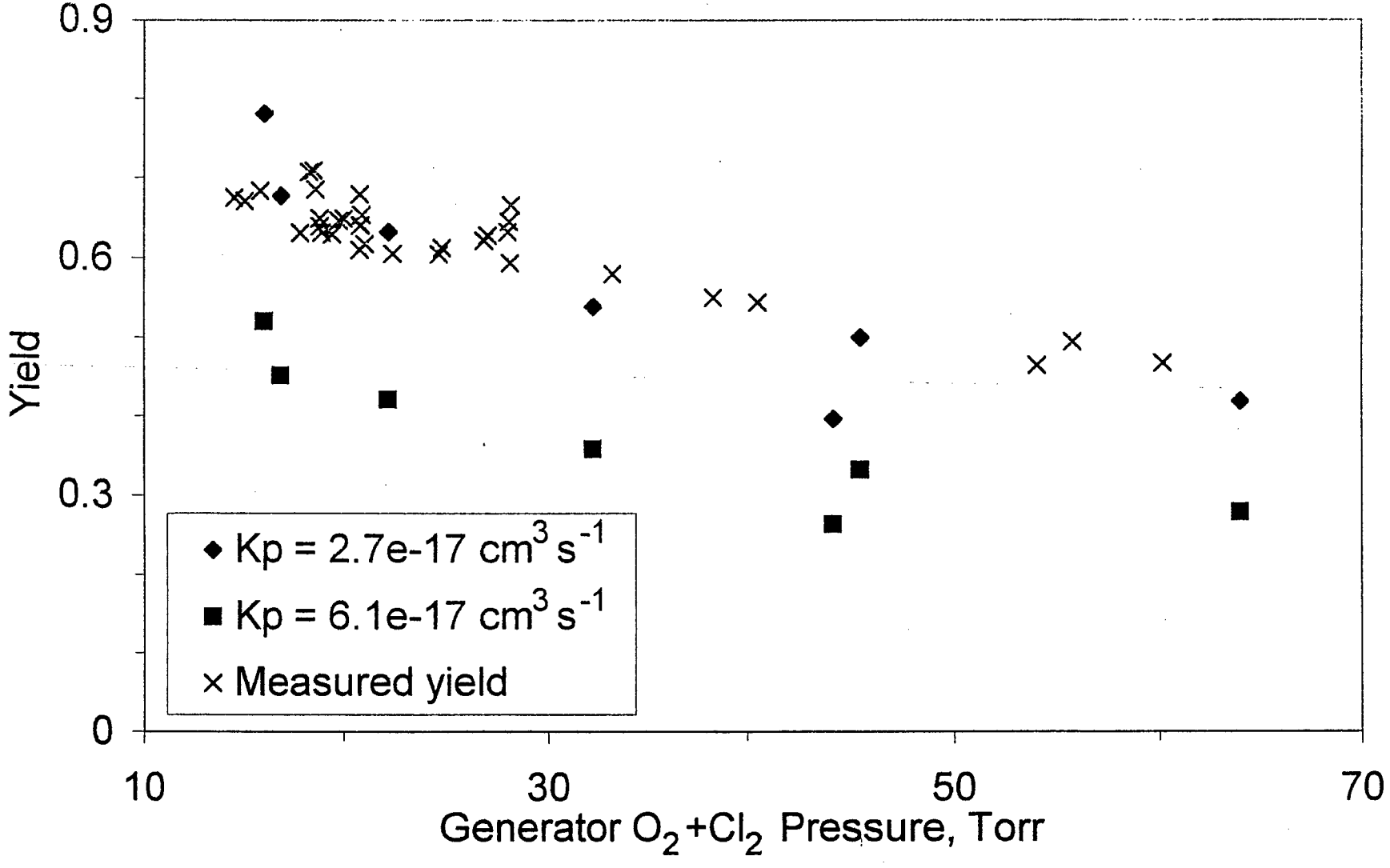

Fig. 12. D. Furman et al. IEEE JQE